NEUTRON SPECTROSCOPY OF ^{22}N AND THE DISAPPEARANCE OF THE N = 14 SHELL

By

Michael J. Strongman

A THESIS

Submitted to
Michigan State University
in partial fulfillment of the requirements
for the degree of

MASTER OF SCIENCE

Physics

2011

ProQuest LLC.
789 East Eisenhower Parkway
P.O. Box 1346
Ann Arbor, MI 48106 - 1346

ABSTRACT

NEUTRON SPECTROSCOPY OF ^{22}N AND THE DISAPPEARANCE OF THE N = 14 SHELL

By

Michael J. Strongman

The emergence of new “magic” numbers in the light neutron-rich oxygen isotopes has led to interest in spectroscopy of other neutron-rich elements like nitrogen. One such nucleus is the $N = 15$ isotope ^{22}N. An excited state of ^{22}N unbound with respect to neutron emission was observed in a stripping reaction from a 85 MeV/u ^{26}F beam. The observed decay energy of 650(50) keV places the level, which is interpreted to be the first 3^{-} state, at an excitation energy of 1.93(22) MeV. Together with the previously measured bound states of ^{22}N, a reduction of the $N = 14$ shell gap compared to less neutron-rich nitrogen isotopes at the neutron dripline is observed. Based on the magnitude of the reduction of the shell gap for ^{22}N, a disappearance of the gap and even a level inversion of the $\nu 1s_{1/2}$ and the $\nu 0d_{5/2}$ levels in the neutron-unbound nucleus ^{21}C seems likely.

Dedicated to my brothers, Kevin and Kyle. I wish both of you the fullest success in your endeavors.

ACKNOWLEDGMENT

Any good Master's Thesis begins with an advisor, and I had the good fortune to get one of the best advisors around, Michael Thoennessen. Thanks for taking a chance on me and encouraging me to see this to the end.

Thank you to my co-advisor, Artemis Spyrou, who has been an excellent guide through this process. I'd also like to thank the third member of my thesis committee, Filomena Nunes, who taught me that theory is always important, even for experimentalists.

I would like to thank the members of the MoNA collaboration. Without them, there would be no MoNA, no experiments, no one to explain how anything works, no captive audience when I'm trying to explain my work, and no one to take on the all important graveyard shifts. Within the group, I'd like to specifically acknowledge the contributions of Warren Rogers, Thomas Baumann, and Paul DeYoung. They managed to teach me practically everything I know about nuclear instrumentation, as well as the art of figuring out seemingly unsolvable problems. Warren was also successful in getting me into nuclear physics in the first place, an achievement that I am immensely grateful for. Calem Hoffman deserves special mention because he lent me the data for thesis experiment, and allowed me to use his calibrations and simulations, as well as answering my questions about analysis.

My work would not have been completed without the help of my fellow graduate students. Shea Mosby and Greg Christian patiently answered my numerous questions about programming and ROOT, even questions I had asked many times already. Special thanks to Michelle Mosby for being a great colleague as well as an excellent baker; your goodies helped fuel the late night work during our experiments. Jenna Smith and Jesse Snyder have been fabulous co-workers and colleagues and I ask them to forgive me for everything I haven't explained about the data acquisition. Phil Voss, Rhiannon Meharchand, Krista Meierbachtol, and Greg Pang deserve special mention for being terrific peers in graduate work, and have all given me good advice and knowledge to navigate the process of defending my thesis.

I would like to extend a special thanks to the families at University Reformed Church that adopted me as their own: Judy and Gerry Gothro, Steve and Marilyn Herwaldt, Tim and Sue Herwaldt, Lee and Joella Cogan, Bruce and Jan Jeffries, Billy and Margie Yang, Dave and Amity Hinkly, and Peeter and Carolyn Lukas. Without you, my mother's fears that I would starve probably would have come true, and your willingness to take me into your family gatherings for the holidays helped stem the tide in the battle of homesickness.

My thanks to my friends in Michigan, Steph, Laura, Brad, Ben, and Eric, who have been supportive in their prayers, and helped out in the tough parts by making me laugh.

I've really appreciated the support of Megan Phillips, Hilary Hayes, and Melissa McLeod. Megan edited the many drafts of my paper, and provide a safe-haven in Santa Barbara when I wanted to see the ocean. Hilary has been a devoted listener and caring friend. And a long distance thanks goes to Melissa, for continuously updating me on her life in China and challenging me to get my degree done.

Of course the final acknowledgement goes to my parents, Ken and Melissa. Dad, finishing your law degree and passing the bar exam has been a great source of inspiration for me. Mom, you have always been my most tireless supporter, my initial cheerleader, and my best critic. Thanks for listening on the phone when I was discouraged, and for doing every chore that I should have been doing while I was at home these past few years.

TABLE OF CONTENTS

LIST OF TABLES

LIST OF FIGURES

Chapter 1

Description of the Problem and Theoretical Foundation

1.1 Introduction

The earliest studies of the structure of nuclei have revealed that for certain “magic” numbers of neutrons and protons, nuclei exhibit more stable behavior than neighboring nuclei, as shown in Fig. 1.1. These magic numbers are 2, 8, 20, 28, 50, 82, and 126. This understanding has explained, for example, the preponderance of stable isotopes at $N = 50$ (^{86}Kr, ^{87}Rb, ^{88}Sr, ^{89}Y, ^{90}Zr, and ^{92}Mo) and the spherical nature of such doubly magic nuclei as ^{48}Ca and ^{16}O.

These magic numbers were assumed to be the same for all nuclei, even as the limits of stability were approached. For example, all $N = 20$ nuclei were assumed to all have large gaps between the highest occupied and lowest unoccupied orbital. Experiments in the late 1970’s [32, 37] cast doubt on whether these gaps are universal throughout the chart of the

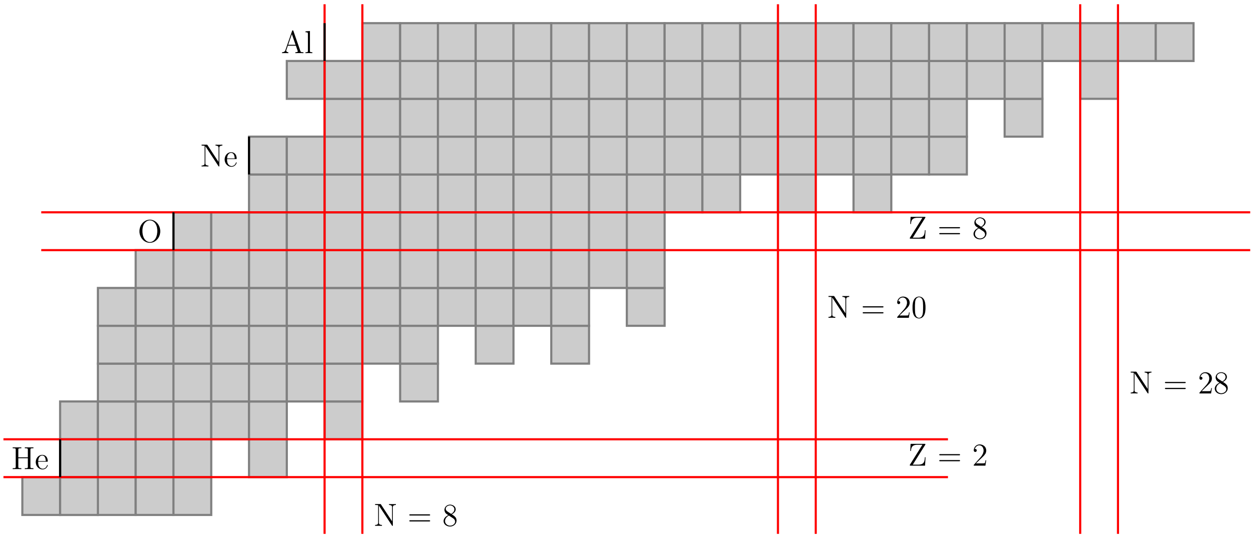

Figure 1.1: The chart of the nuclides for $Z \leq 13$. The red lines denote the traditional "magic" numbers for this region. (For interpretation of the references to color in this and all other figures, the reader is referred to the electronic version of this thesis.)

nuclides by showing that ^{31}Na and ^{32}Na do not have the expected mass excess of a magic nucleus. This so-called "island of inversion" [34], shown in Fig. 1.2, is the first of several "islands of shell breaking" [6] where the traditional understanding of the shell model breaks down and new, unexpected properties of nuclei emerge. In respect to this thesis, the light neutron rich isotopes of oxygen, nitrogen, and carbon, shown in Fig. 1.3, exhibit these new properties. To investigate the shell model in this region, information on the excited levels of isotopes need to be measured.

1.2 The Nuclear Shell Model

The main theoretical model that has been utilized to understand the structure of nuclei and explain the emergence of magic numbers has been the Shell Model. Since describing the nucleus with the motion of each nucleon is a many body problem and thus non-solvable, approximations have to be made. The underlying idea behind the Shell Model is that the

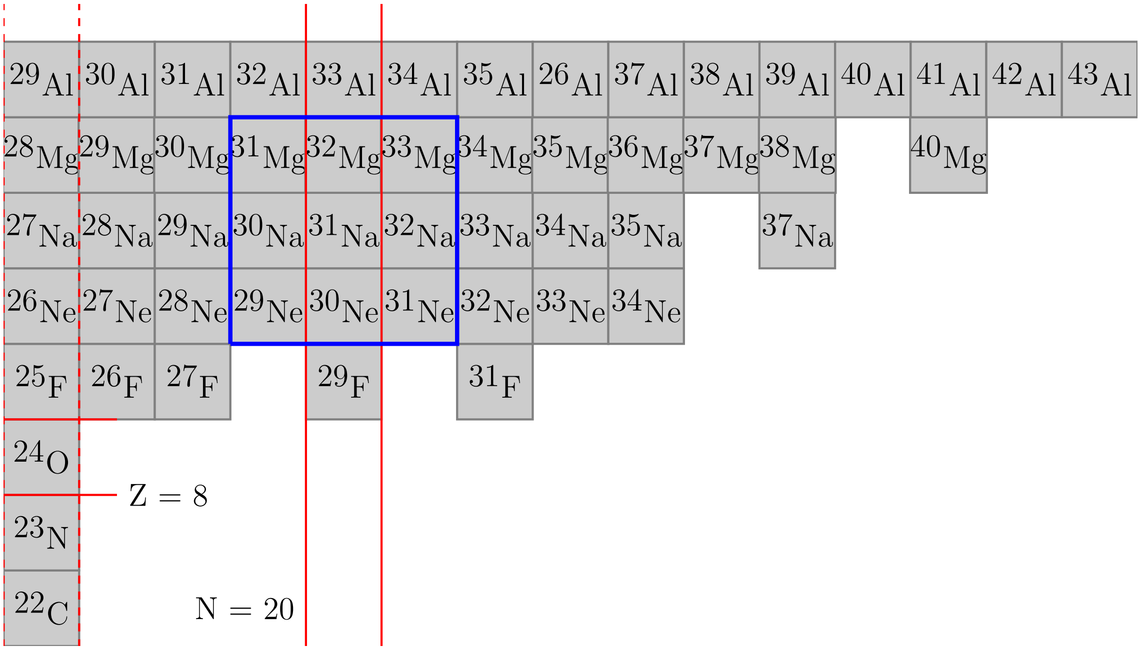

Figure 1.2: A close up of the region in the nuclides containing the “island of inversion”, highlighted by the blue outline. Isotopes in this region do not have the expected properties of “magic” nuclei for the $N = 20$ closure.

interactions of a single nucleon with the rest of the individual nucleons inside the nucleus can be approximated by an overall mean field [16]. Thus, the energy levels of the nuclei can be calculated using a single central mean potential, just like in atomic physics for electrons.

Within the Shell Model, the orbitals in which nucleons are occupied are labeled in the similar manner as for atomic orbitals, according to the quantum numbers n, ℓ, and J. n is the principal quantum number.[1] ℓ is orbital angular momentum. J is total angular momentum calculated by adding the intrinsic spin of the nucleon to ℓ. Therefore, J is either $\ell + \frac{1}{2}$ or $\ell - \frac{1}{2}$. Shorthand for labeling the orbitals by quantum number goes as nL_J, where n is the principal quantum number, L is a letter that corresponds to ℓ,[2] and J is the total angular momentum. The occupation number of a particular orbital can be calculated from

---

[1] In this description we choose to start the n at 0.

[2] s: $\ell = 0$, p: $\ell = 1$, d: $\ell = 2$, and f: $\ell = 3$

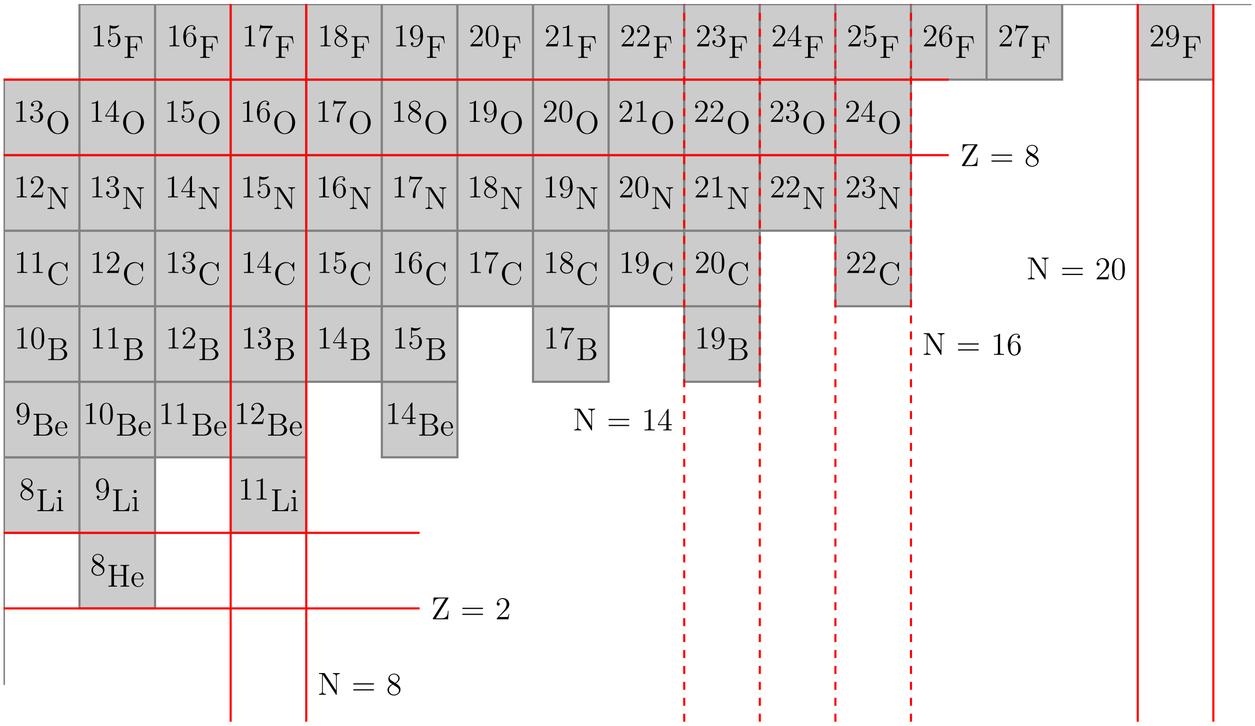

Figure 1.3: A close up of the neutron rich region of interest within the chart of the nuclides. The red lines mark the traditional shell closures in this region: $N = 8$, $N = 20$ and $Z = 2$ and $Z = 8$. The red dashed lines mark the "new" magic numbers ($N = 14$ and $N = 16$) which emerge in the neutron rich isotopes of this region.

$2J+1$. Therefore, an orbital with $n=0$, $\ell=2$ and $J=5/2$ is labeled as $0d_{5/2}$ and has an occupation number of $2\times 5/2+1=6$.

Each orbital has an Effective (spherical) Single Particle Energy (ESPE or SPE). This is a measurement of the mean effect of other nucleons on the single particle orbit. Two body matrix elements (TBME) depend on J, T coupled by j_1, j_2 interacting nucleons and are used to calculate the interaction of a nucleon of $J=j_1$ on a nucleon of $J=j_2$. These two physical parameters are taken empirically from fits to experimental data.

1.2.1 History of the first "magic" numbers

It was first observed in the late 1940's that nuclei with neutron or proton numbers of 20, 50, 82, or 126 are particularly stable. This behavior wasn't explained by the traditional Wood-Saxon Potential:

$$V(r)=\frac{V_0}{1+\exp{(r-R)/a}} \tag{1.1}$$

In 1949, a solution was proposed by Mayer [19, 20], Haxel, Jensen, and Suess [11] which involved adding a correction to the mean field: the spin-orbit force. The spin-orbit force splits orbits with the same angular momentum ($\vec{\ell}$) into j-lower ($j_<$) and j-upper ($j_>$) total angular momenta.

The spin orbit potential is:

$$V_{SO}=-\frac{1}{r}\frac{dV(r)}{dr}\vec{\ell}\cdot\vec{s} \tag{1.2}$$

where $\vec{\ell}$ is the orbital angular momentum and $\vec{s}$ is the intrinsic spin angular momentum of the nucleon.

If we apply the $\vec{\ell} \cdot \vec{s}$ term of spin-orbit to a state with total angular momentum of $\ell + 1/2$:

$$< \psi_{j=\ell+1/2} | - \vec{\ell} \cdot \vec{s} | \psi_{j=\ell+1/2} >= -\frac{\ell}{2} \tag{1.3}$$

and $\ell - 1/2$:

$$< \psi_{j=\ell-1/2} | - \vec{\ell} \cdot \vec{s} | \psi_{j=\ell-1/2} >= +\frac{\ell+1}{2} \tag{1.4}$$

We see that the spin-orbit force splits the degeneracy of levels corresponding to the same ℓ. When added to the traditional mean field of a Wood-Saxon potential, we noticethat the magic numbers observed emerge. This explains the magic numbers above $N = 20$.

1.2.2 Calculations with the Shell Model

Because using the whole model space of all possible quantum numbers makes calculations of energy states cost prohibitive, physicists typically truncate the model space to fit the particular nucleus that is being calculated. A model space corresponds to all the combined shells that nucleons are allowed to occupy for a given calculation. For example, calculations of the neutron rich oxygen isotopes are typically truncated to the *sd* shell ($0d_{5/2}$,$1s_{1/2}$, and $0d_{3/2}$) and assume an ^{16}O core (that is, it assumes that the nucleons that fill the $0s$ and $0p$ are effectively inert and the contributions of orbitals above the $1s$ and $0d$ are negligible). Each subset of the model space has empirically defined Hamiltonians consisting of different ESPEs (Effective Single-Particle Energies) and TBMEs (Two-body Matrix Elements).

For neutron rich isotopes with $Z \geq 8$, the USD interaction [36] is used to calculate excitations within the *sd* only. Excitations to higher orbitals, like the *pf* shell, are ignored. This uses a model space of exclusively the *sd* shell assuming an ^{16}O core. The interaction

Hamiltonian	Model Space	Source
USD	*sd* with ^{16}O core	[36]
WBT	*spsdpf* with no core	[35]
WBP	*spsdpf* with no core	[35]

Table 1.1: The Hamiltonians used to calculate the level energies in this thesis.

is defined by 63 TBMEs and 3 single particle energies (SPE) for each orbit in the *sd* space ($0d_{5/2}$,$1s_{1/2}$, and $0d_{3/2}$). This Hamiltonian dates from 1983 and has been the dominant interaction used for nuclei with masses $A = 18$ to $A = 38$. The TBME and SPE for the USD are obtained from a least square fit of 447 binding energies and excitation energies of *sd* shell nuclei [35]. For the *sd* shell the TBMEs are scaled as follows: $TBME^{A} = TBME^{A=18} \times \frac{A}{16}^{0.3}$ [35].

In order to calculate carbon and nitrogen nuclei, the WBT and WBP interactions are needed because a ^{16}O core is unreasonable and interactions with the $\pi 0p_{1/2}$ shell are necessary for the protons. These Hamiltonians are active in a full *spsdpf* model space (which will include the TBMEs of the USD interaction). The difference between the two interactions is that they use different choices of least-squares fitting of the experimental energies for the SPE and TBME. The WBT uses a fitting of linear combinations of the effective TBMEs with some parameters normalized by the G-matrix method [35]. The WBP uses the modified surface one boson exchange method to achieve similar fits of TBMEs [35]. Both interactions produce similar results for stable nuclei, and for reasons described in Sec. 4.1, both will be used.

1.3 Evolution of Magic Numbers in neutron-rich nuclei

New magic numbers and shell gaps have arisen for neutron rich nuclei, in particular for the oxygen isotopes. The first evidence that this might be the case came from investigation of the systematics of the neutron separation energies (S_n) as a function of isospin [12]. Experiments investigating the region near $N = 16$ have confirmed the emergence of a new magic number. Evidence includes the lack of bound excited states for ^{23}O and ^{24}O [29], the high energy excited states populating the $\nu 0d_{3/2}$ shell in ^{23}O [9], the spherical content of the ^{24}O ground state [15], the high first and second unbound excited states of ^{24}O [14], and the unbound state energy of ^{25}O [13]. Furthermore, since the neutron drip line has been confirmed for $Z < 9$, the fact that three neighboring elements (carbon, nitrogen, oxygen) have the same neutron number for the last bound nucleus [22], dramatically points to a solid shell closure of $N = 16$.

Another new magic number is $N = 14$ which was first observed in ^{22}O. The properties of ^{22}O that was the evidence for this included the high excitation energy of the first excited 2^+ state [33, 3, 29] and the low B(E2) value of the 2^+ state [33].

The $N = 14$ shell gap develops in the oxygen isotopes due to the attractive monopole matrix element $V^{\mathrm{nn}}_{d_{5/2}d_{5/2}}$ as neutrons fill the $\nu 0d_{5/2}$ orbit, increasing the binding relative to the $\nu 1s_{1/2}$ orbit [28]. This is exhibited in Fig. 1.4 by the gradual decline in ESPE of the $\nu 0d_{5/2}$ shell from $N = 8$ to $N = 14$. Also the $V^{\mathrm{nn}}_{s_{1/2}\ d_{3/2}}$ is slightly repulsive, adding to the effect. However, as neutrons fill the s orbit, between $N = 14$ and $N = 16$, a similar attractive force ($V^{\mathrm{nn}}_{s_{1/2}\ s_{1/2}}$) reduces the ESPE of the $\nu 1s_{1/2}$ orbit.

The gap between the $\nu 1s_{1/2}$ and $\nu 0d_{5/2}$ is predicted to be largest for ^{22}O and will decrease with increasing distance from ^{22}O. In the carbon isotopic chain, reducing the number

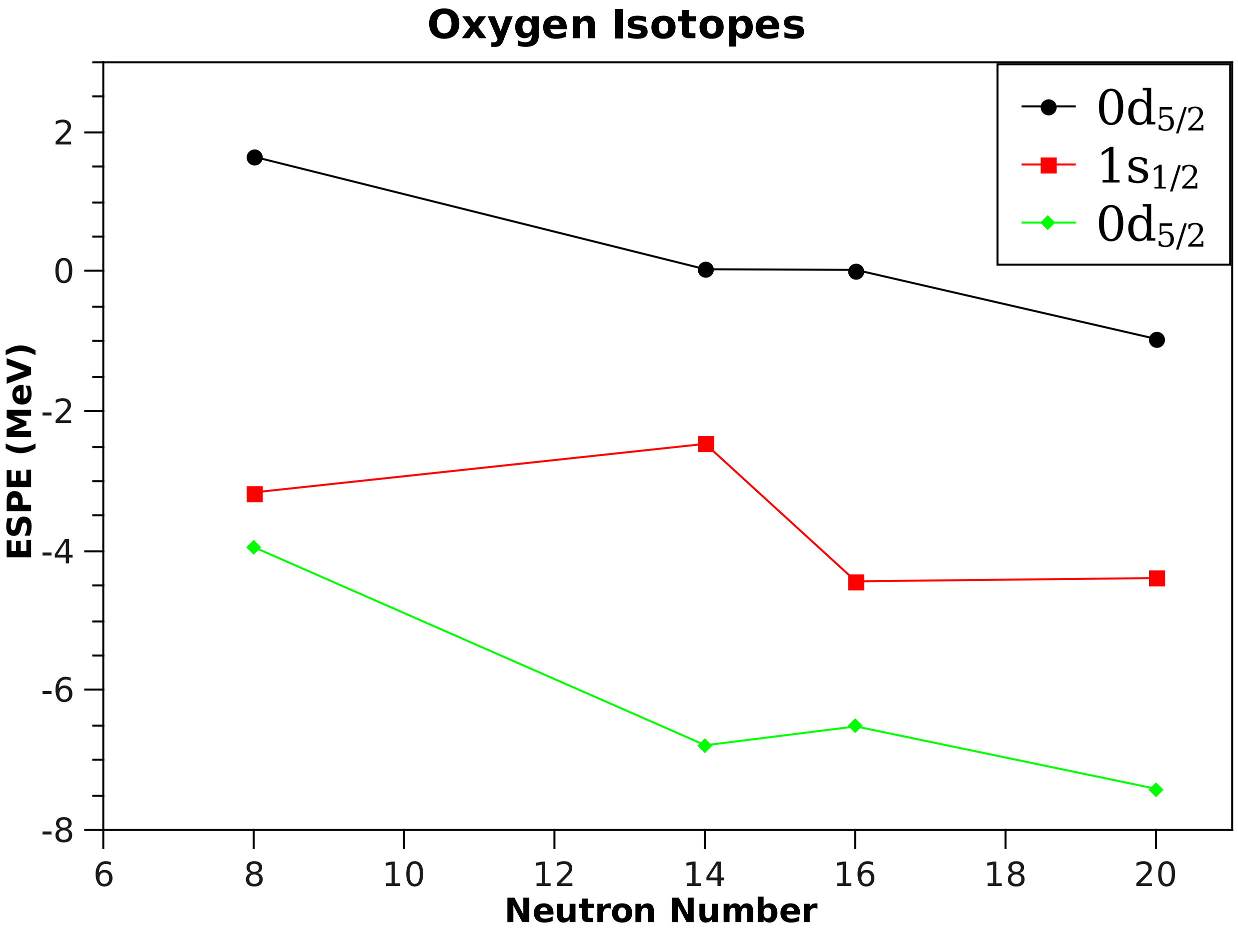

Figure 1.4: The evolution of the *sd* shell gaps of oxygen isotopes as function of neutron number using the USD interaction from Ref. [36].

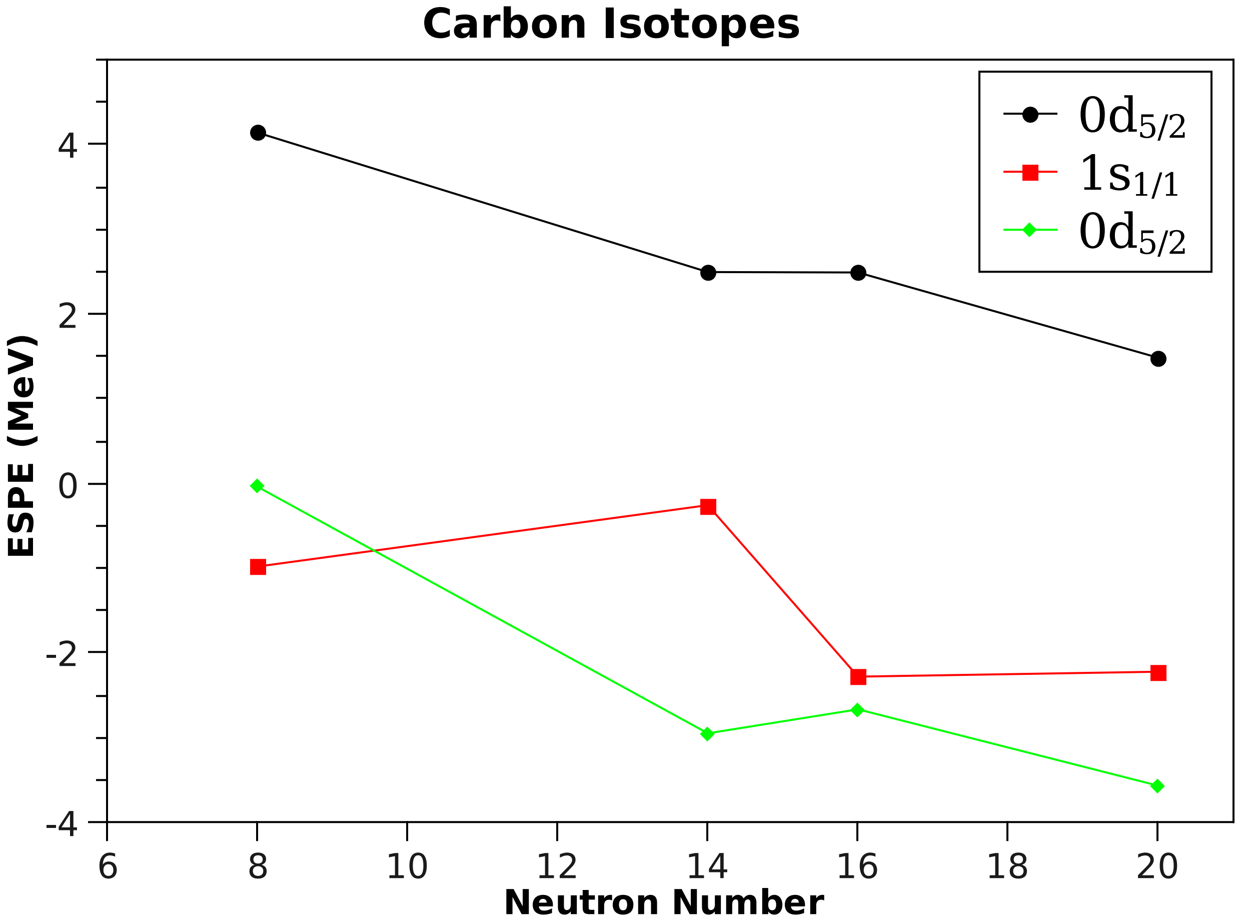

Figure 1.5: The evolution of the *sd* shell gaps of carbon isotopes as a function of neutron number using the WBT interaction from Ref. [35]. Note the inversion of the $\nu 1s_{1/2}$ and $\nu 0d_{5/2}$ shells as the number of neutrons are reduced from 14 to 8.

of neutrons from ^{20}C ultimately leads to the inversion of the $\nu 1s_{1/2}$ and the $\nu 0d_{5/2}$ levels as shown in Fig. 1.5. A similar inversion is possible as neutrons are added to ^{20}C.

These effects happen for the oxygen isotopes but not for higher Z isotopes because the $V_{\pi j>\nu j<}$ (the potential between a proton and neutron with the same ℓ but opposite spins) is attractive so as protons fill the $\pi 0d_{5/2}$, the orbit just above $\nu 0d_{5/2}$ (the $\nu 1s_{1/2}$) goes down in energy.

The question remains as to if the $N = 14$ shell gap persists for $Z < 8$. We know from the level inversion at ^{15}C [31] that the $\nu 0d_{5/2}$ shell starts above the $\nu 1s_{1/2}$ for $N = 8$ as seen in Fig. 1.5. The same attractive matrix element for $\nu 0d_{5/2}$ acts in the carbon isotopes as in the oxygen isotopes, so the $\nu 0d_{5/2}$ is expected to drop in energy, however, the question remains where the $\nu 0d_{5/2}$ will lie in energy relative to the $\nu 1s_{1/2}$.

1.4 Extracting shell gaps from single particle states

The evolution of a shell gap with a neutron number N can be extracted from single particle or single hole levels in the $N-1$ or $N+1$ nuclei. The difference in energy between two orbitals can be determined via the prescription of Lawson and Uretsky [17]. Their center of gravity theorem displayed in Eqn. 1.5 shows that the weighted average of excited states that correspond to a configuration reasonably estimates the energy between two orbitals.

$$E = \frac{\sum_J (2J+1)E_J}{\sum_J 2J+1} \tag{1.5}$$

An example of this would be measuring the gap between the $\nu 1s_{1/2}$ and $\nu 0d_{5/2}$ in ^{22}O. The ground state of the ^{22}O is a filled $\nu 0d_{5/2}$ shell as shown in Fig. 1.6. The first two

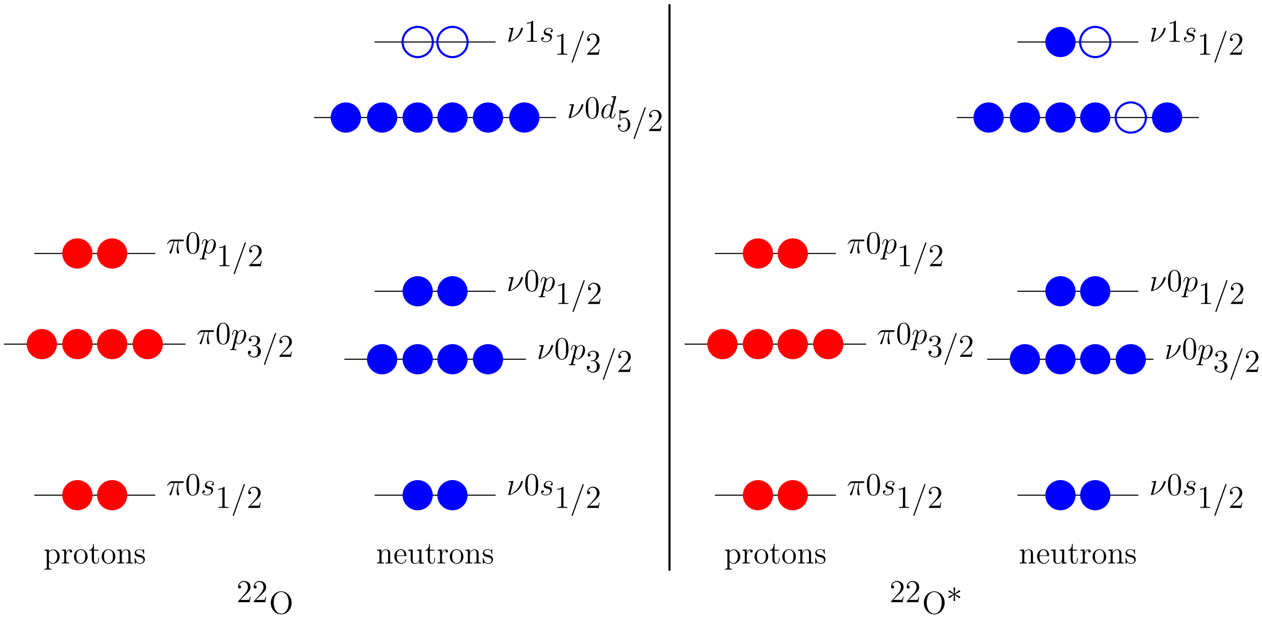

Figure 1.6: The shell configuration for the ground state of ^{22}O (left) and the first excited states of ^{22}O (right). Closed circles represent nucleons occupying the orbital while open circles are positions where a nucleon could occupy. The gaps between shells are not to scale.

excited states were identified (with guidance of the shell model) to be 2^+ at 3.199 MeV and 3^+ at 4.582 MeV [29]. Performing a weighted average as follows:

$$E = \frac{(2 \times 2 + 1)3.199 \text{ MeV} + (2 \times 3 + 1)4.582 \text{ MeV}}{(2 \times 2 + 1) + (2 \times 3 + 1)} = 4.2 \text{ MeV} \tag{1.6}$$

This result agrees well with the predicted gap of 4.3 MeV from the USD [8, 29]. More complicated configurations, where both the lower shell and higher shell have multiple J combinations, simply require adding all the relevant states.

This approach for estimating shell gaps from weighted averages of excited states was used by Talmi and Unna [31] to predict the inversion of the $\nu 1s_{1/2}$ shell in ^{11}Be. Fig. 1.7 shows the linear extrapolation of the gaps in ^{13}C and ^{12}Be to the gap in ^{11}Be.

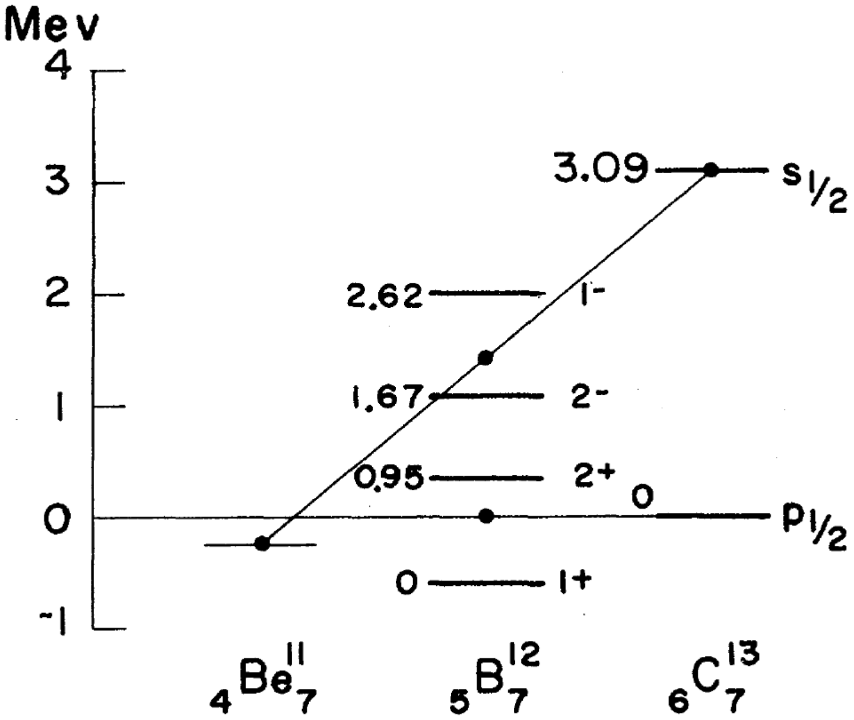

Figure 1.7: The "competition" of the $1s_{1/2}$–$0p_{1/2}$ shells in N = 7 isotones from Ref. [31]. These are the calculated shell gaps for $6 \geq Z \geq 4$.

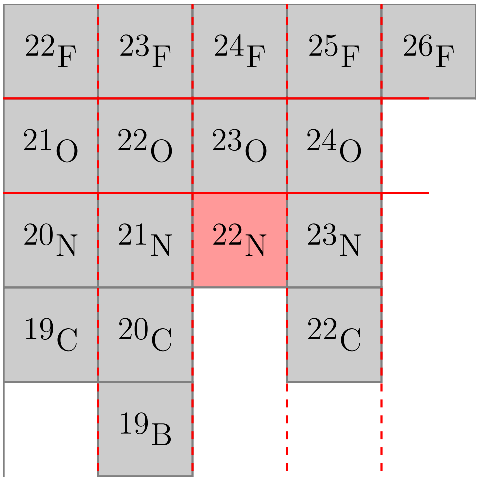

Figure 1.8: An inset of the region of nuclei around the $N = 14$ shell closure. The isotope of interest in this thesis (^{22}N) is highlighted in red.

1.5 Experimental Studies of $N = 14$ Shell Gap

The size of the gap between $\nu 1s_{1/2}$ and $\nu 0d_{5/2}$ orbitals has been determined for the $N = 14$ nucleus ^{22}O [29]. Stanoiu *et. al.* determined that the gap is 4.2 MeV from measurements of the 2^+ and 3^+ excited states of ^{22}O. The $Z = 7$ isotone of ^{22}O, ^{21}N, was measured using gamma ray spectroscopy. Because the proton shell is not closed for nitrogen isotopes, more states are needed to calculate the shell gap. Sohler *et. al.* measured and identified the four excited states corresponding to the same orbits as the 2^+ and 3^+ in ^{22}O. Using the same prescription as Lawson and Uretsky [17], Sohler *et. al.* [27] found an estimated shell gap of 3.03 MeV, a one MeV reduction of $N = 14$ shell gap, and concluded that there is a partial survival of the magicness of $N = 14$ for the nitrogen isotopes.

The size of the gap between $\nu 1s_{1/2}$ and $\nu 0d_{5/2}$ orbitals has been determined for the $N = 15$ nucleus ^{23}O [26]. The spin and parity of the ground state of ^{23}O is $1/2^+$ (a $\nu 1s_{1/2}$ particle state) and thus the measurement of the $5/2^+$ excited state (a $\nu 0d_{5/2}$ hole state) at 2.79(13) MeV directly determines the size of the gap between the $\nu 1s_{1/2}$ and $\nu 0d_{5/2}$

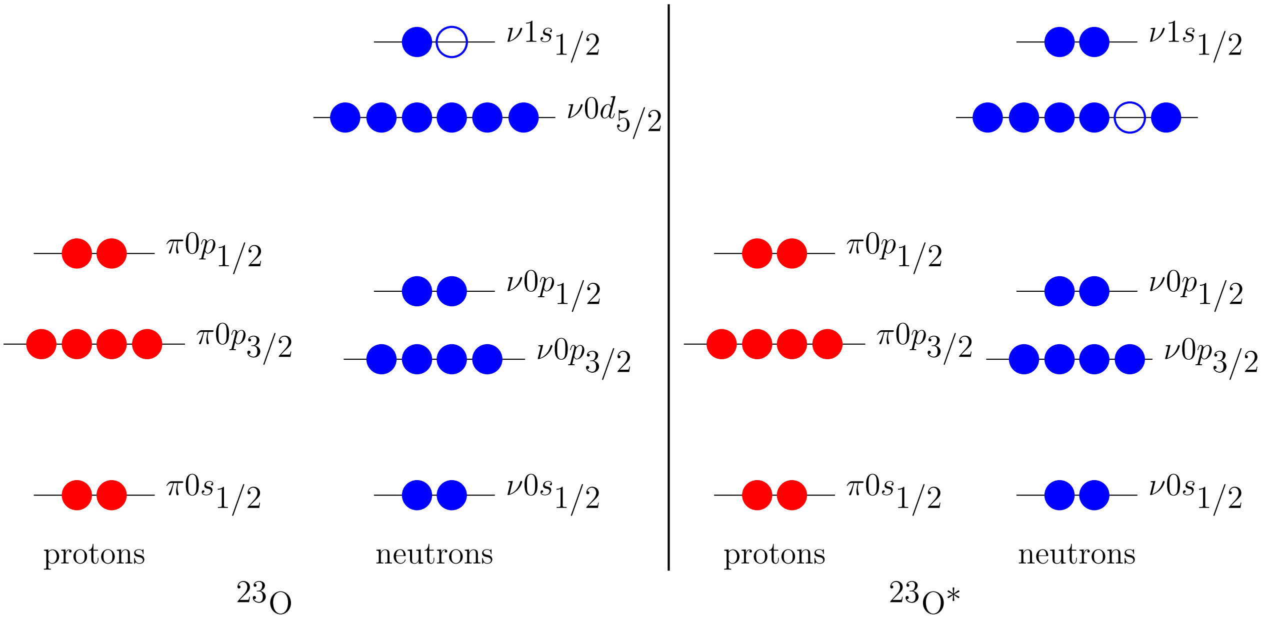

Figure 1.9: The shell configuration for the ground state of ^{23}O (left) and the first excited state of ^{23}O (right). Closed circles represent nucleons occupying the orbital while open circles are positions where a nucleon could occupy. The gaps between shells are not to scale.

orbitals as shown in Fig. 1.9.

To perform the same analysis for the $N = 15$ nucleus ^{22}N, shown in relation to the isotopes mentioned above in Fig. 1.8, more states are needed. Because the last proton shell for nitrogen isotopes is not closed, the $\nu 1s_{1/2}$ particle and $\nu 0d_{5/2}$ hole states are coupled to a $\pi 0p_{1/2}$ state (shown in Fig. 1.10). The ground state of ^{22}N is assigned a spin and parity of 0^- and the first excited state is 1^-. Both correspond to the $\nu 1s_{1/2}$ particle states, coupled to $\pi 0p_{3/2}$ shell for protons. The states that correspond to the $\nu 0d_{5/2}$ hole state are 2^- and 3^-.[3] Measurements of all three excited states (1^-, 2^-, and 3^-) are necessary to determine the $1s_{1/2}$–$0d_{5/2}$ shell gap and study the shell evolution of $N = 15$ nuclei.

---

[3] Guided by the shell model

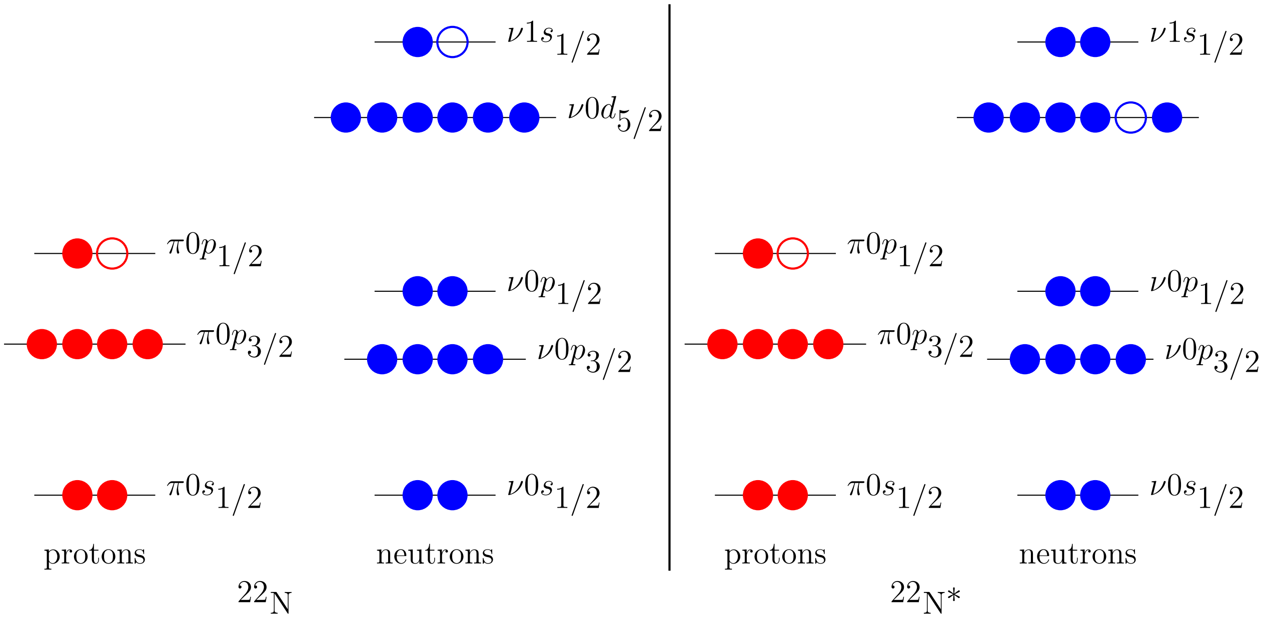

Figure 1.10: The shell configuration for the ground state of ^{22}N (left) and the first excited states of ^{22}N (right). Closed circles represent nucleons occupying the orbital while open circles are positions where a nucleon could occupy. The gaps between the shells are not to scale.

1.6 Previous Measurements of ^{22}N

A neutron knockout experiment of ^{22}N was carried out at the Fragment Separator at GSI Darmstadt. Rodriguez *et. al.* [24] measured the momentum distributions of neutron knockouts from several neutron-rich nuclei, including $^{16-22}$N, $^{19-23}$O and $^{21-26}$F. Of interest here are their results of ^{22}N. The experimenters deduced from the larger cross section and small width of the longitudial-momentum for ^{22}N that there is a change from a $0d_{5/2}$ to $1s_{1/2}$ valance neutron. This is an effect already observed for ^{23}O and ^{24}F, and expected for isotopes above $N = 14$. This is consistent to the shell model (see Fig 1.4 and Fig 1.5) that the $\nu 1s_{1/2}$ is above the $\nu 0d_{5/2}$. Therefore, the assignment of the ground state of ^{22}N to a spin-parity of 0^- is justified and higher excited states are expected from the spinflip pair of 0^- (1^-) and $\nu 0d_{5/2}$-hole states (2^- and 3^-) respectively.

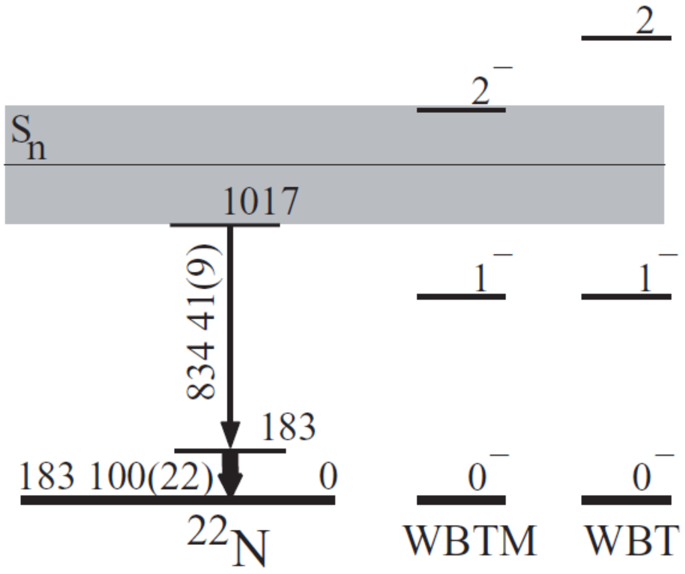

Figure 1.11: The measured level scheme of ^{22}N from Ref. [27]. The 1^- and 2^- are the first two excited states predicted by the shell model so the 183 KeV and 1017 keV state are assigned these spin-parity respectively.

Solher *et al.* [27] performed gamma ray spectroscopy of the neutron-rich nitrogen isotopes including ^{22}N at GANIL. Since the gamma rays of 183 keV and 834 keV of energy were in coincidence,they attributed this to a gamma cascade from a 1.017 MeV state to a 183 keV state. With guidance from the shell model, the first and second excited states were identified as 1^- and 2^- respectively. Figure 1.11 shows the level scheme of ^{22}N. Since Sohler did not observe any other gamma rays, any higher excited states are assumed to be neutron unbound and higher than the neutron separation energy of 1.28(22) MeV. Therefore, it is necessary to perform neutron spectroscopy experiments to measure any higher lying states.

Chapter 2

Experimental set-up

Neutron spectroscopy experiments involve the reconstruction of a neutron unbound state from its decay products. The unbound states are populated from various reactions, such as one-proton knockout and multiple-neutron evaporation from a rare isotope beam. One neutron spectroscopy experiment was performed in the summer of 2005 involving a ^{26}F rare isotope beam, which was designed to measure the neutron unbound ground state of ^{25}O, the results of which have already been published in [13] and [12]. Decays of ^{22}N were also observed in this experiment.

The experiment was carried out with the MoNA-Sweeper set-up in the N4/N6 vault at the National Superconducting Cyclotron Laboratory (NSCL). A primary beam of ^{48}Ca accelerated to 140 MeV/nucleon impinged on a 987 mg/cm^2 Beryllium target. Isotopic selection of ^{26}F was achieved with the A1900 fragment separator [21]. The beam energy was 85 MeV/nucleon and contained other constituents including a factor of 100 more ^{29}Na. A 5 mm thick plastic timing scintillator was located at the end of the A1900 fragment separator to allow the constituents of the beam to be separated by time-of-flight.

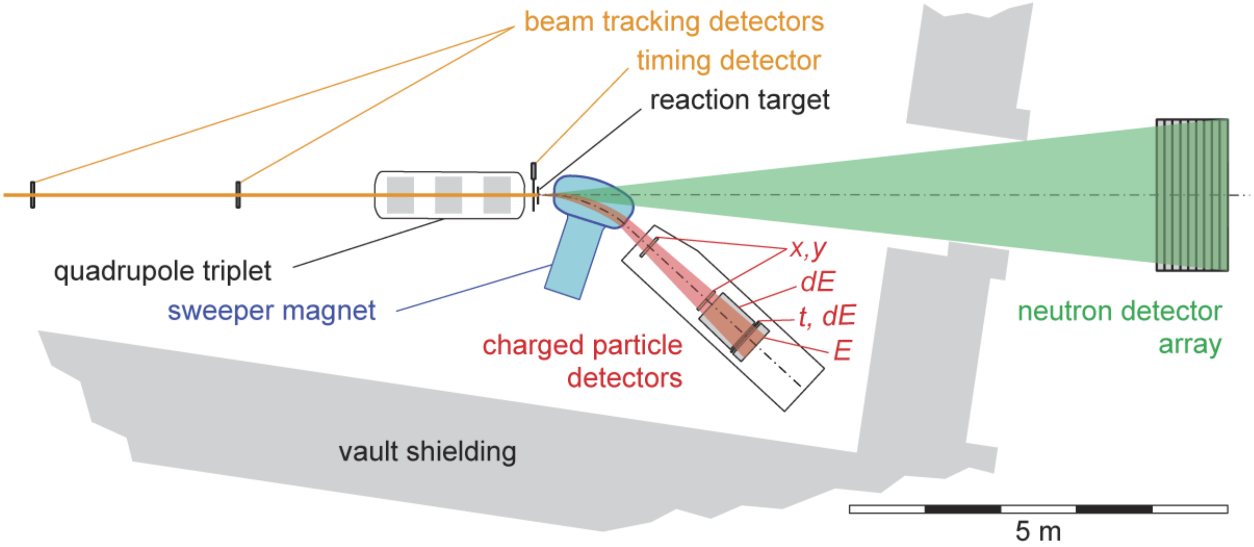

Figure 2.1: The experimental setup for the MoNA-Sweeper for experiment 05039. MoNA is the neutron detector array in green (right) and Sweeper dipole magnet is in blue, located after the reaction target. Figure taken from Ref. [12].

The beamline between the A1900 and the target position had two position sensitive parallel-plate avalanche chambers (PPACs), located 3.97 m upstream of the target, as well as a focusing triplet magnet. The PPACs measured the spatial characteristics of the incoming beam. 6.25 cm before the target position was a 0.254 mm plastic timing scintillator that provided timing information of the beam. The target consisted of 470 mg/cm^2 of Beryllium.

2.1 The Sweeper Focal Plane Detectors

After the neutron unbound nucleus decays, the energy and momenta of the neutron and the leftover fragment are measured, because they are required in order to reconstruct the decay energy.

The expelled charged fragments from the reaction are sent through a large gap dipole magnet (Sweeper) [4] that deflected these fragments 43° into the focal plane charged-particle detectors. Any neutrons produced in the reaction are not deflected, pass through the large gap in the dipole, and are detected by the Modular Neutron Array (MoNA) [2] at zero degrees 8.2 meters downstream of the target position. Figure 2.1 shows the positions of the Sweeper and MoNA relative the target positions.

After the sweeper magnet, there were two cathode-readout drift chambers (CRDCs) to detect the position of charge fragments leaving the focal plane. These CRDCs, located 1.88 m apart, had 128 pads in the dispersive direction, where a Gaussian position of the charge distribution determines the position. The position in the non-dispersive direction is determined by the time taken to drift to the anode.

Downstream the CRDCs, there is an ion chamber to detect the energy loss of charged fragments. Behind the ion chamber were two plastic scintillators 0.5 cm and 15 cm thick respectively. Each scintillator has two photo-multiplier tubes (PMTs) attached above and below the device. The energy signals of all four PMTs are gain-matched and geometrically averaged to determine the energy of the signal. The thinner scintillator was the trigger for the entire system and served as a secondary measurement of the energy loss of the fragments, here to after known as the dE scintillator. The average of the timing signals for the dE scintillator also served as the absolute timing of fragments exiting the focal plane. The other scintillator measure the total kinetic energy (TKE) of the fragments.

2.2 The Modular Neutron Array (MoNA)

The Modular Neutron Array, shown in Fig. 2.2, consists of 144 $10 \times 10 \times 200$ cm^3 BC-408 plastic scintillator bars [2]. They are arranged in a 16×9 configuration 8.20(5) m from the target and aligned at 0° relative to the beam direction. The size and position of the array allow for an angular coverage of neutrons from $\pm 7.0^\circ$ in the horizontal and $\pm 5.6^\circ$ in the vertical.

Each bar has photomultiplier tubes (PMTs) attached to each end with an accompanying light guide. Neutrons interact with the particles in the plastic (hydrogen or carbon nuclei) and those charged particles become excited and emit photons of light to de-excite. These photons are collected by the PMTs at the ends of each bar which determine the time and charge collected. The time difference between PMT signals at each end is used to calculate the location of the event in the horizontal position within a bar. Vertical position and distance from the target of the interaction is calculated via the position of the bar within the array that detects the event with an uncertainty of ±5.0 m. The time measurement of the event was calculated from the mean time of the PMTs of the bar with the particular hit.

2.3 Calibrations

It should be noted that this experiment was designed to investigate the ground state decay of ^{25}O. The principal investigator for this experiment, Calem Hoffman, performed all the necessary detector calibrations for this experiment.

Calibrations for the Modular Neutron Array were performed by using data collected from cosmic ray muons. Since the fast moving muons scatter off the plastic inside the MoNA bars in the same manner as a neutron, depositing the average electron equivalent of 22 MeV energy in each bar, cosmic data can be used to perform high voltage gain matching for each PMT and energy calibration for each charge-to-digital (QDC) module that interprets the raw PMT charge collected. Time information from the PMTs is collected by time-to-digital (TDC) modules which are calibrated by a pulser device that gives a series of pulses at a known interval. Converting the time difference into a position on the bar requires a

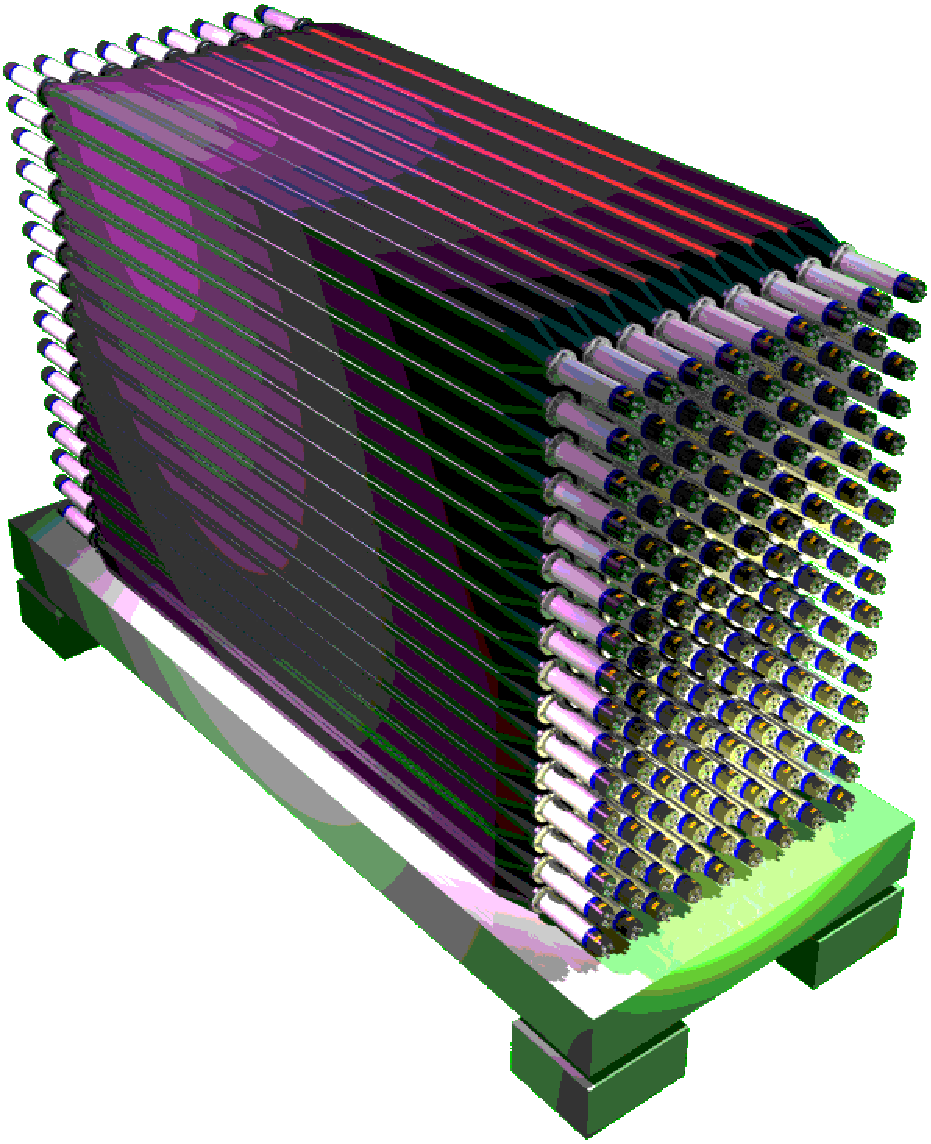

Figure 2.2: The Modular Neutron Array (MoNA), a neutron detector array of 144 plastic scintillating detectors. Figure provided courtesy T. Baumann.

calibration of positions. Because cosmic muons illuminate the bars uniformly, analysis of the time difference spectra for each bar during a cosmic run yields a slope and offset to convert time to a position on the bar.

Calibrations for the charged particle detectors in the beamline and the sweeper focal plane involve gain matching the response of PMTs relative to each other, correcting for the position dependence of the energy deposition on the thin and thick detectors, and doing relative energy calibrations. The position sensitive CRDCs and PPACs are calibrated by placing masks of holes in known absolute positions in front of them as the dispersed beam is sent through the focal plane. Identifying the holes in the position spectra allows for absolute position determination.

A detailed description of these calibrations can be found in Reference [12].

Chapter 3

Analysis of experiment

3.1 Incoming beam identification

The first step of the analysis is to identify the incoming beam. As the incoming beam was not pure but composed of ^{26}F and ^{29}Na as well as some low Z constituents, it is necessary to tag events with the proper incoming beam. The magnetic rigidity of the beam (^{26}F and other constituents) at the end of the A1900 spectrometer was 3.9301 Tm. Because the components of the beam had the same rigidity and different masses, they have different velocities as shown in Table 3.1.

The beam passes through 35.68 m of beam-line between the A1900 scintillator and the timing scintillator, so the ^{26}F is separated by time-of-flight from the ^{29}Na. No target runs

Isotope	Velocity (cm/ns)	time-of-flight (ns)
^{26}F	12.0164	296.9
^{29}Na	12.967	275.2

Table 3.1: The velocities and time-of-flight for the two major components of the incoming beam to travel between the A1900 focal plane to the target.

with the sweeper set to accept the ^{26}F and ^{26}Na were used to identify the relative time-of-flight of the beam. As Fig. 3.1 shows, the ^{26}F is clearly separated from the rest of the beam by time-of-flight. Therefore, by gating on time-of-flight between the A1900 scintillator and the target scintillator (in Fig. 3.2), we isolate the incoming ^{26}F beam.

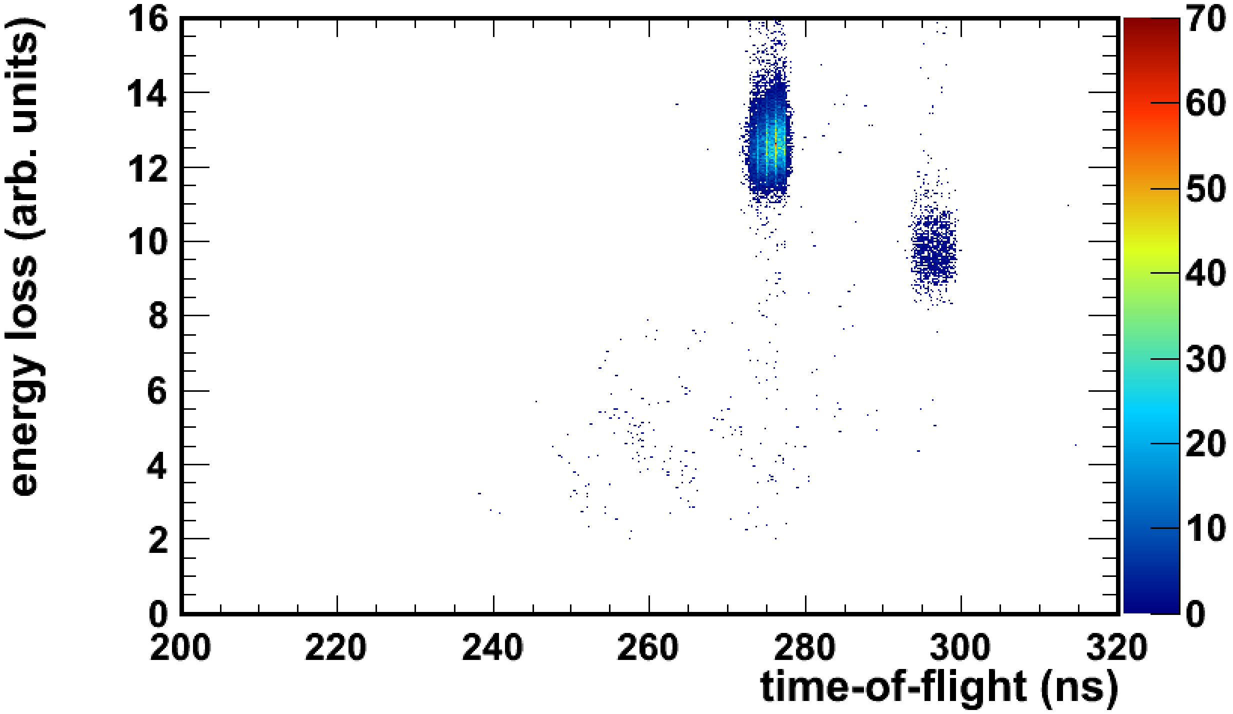

Figure 3.1: Energy loss versus time-of-flight for the beam exiting the A1900 focal plane showing the separated ^{26}F and ^{29}Na.

3.2 Element Identification

Element identification is achieved through measuring the energy loss and total kinetic energy of fragments that travel through the sweeper. Energy loss is measured by the ion chamber and the dE scintillator. The ion chamber has better resolution than the thin scintillator. Total kinetic energy (TKE) is measured by the TKE scintillator.

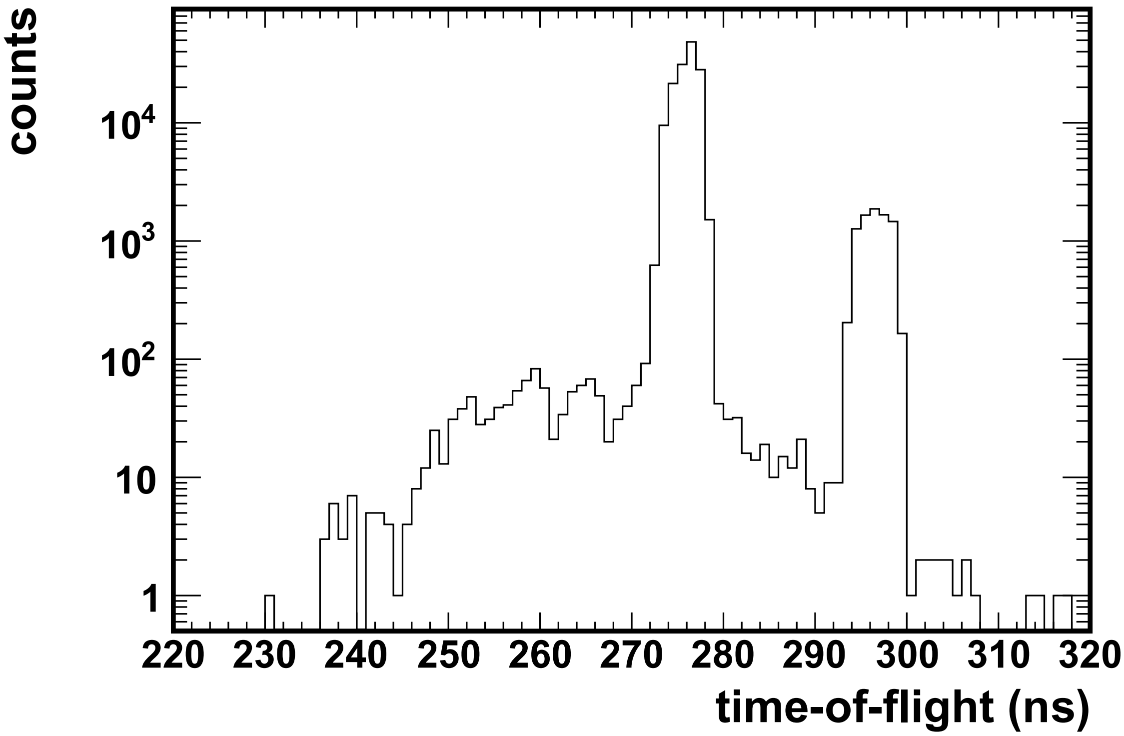

Figure 3.2: The time-of-flight for beam particles traveling from the end of the A1900 focal plane and the target position. The intense peak at 297 ns is the ^{26}F.

Plotting the energy losses in the ion chamber and the dE scintillator gives distinct element identification. The intense section in Fig. 3.4 is the unreacted fluorine beam, therefore, counting down we can identify oxygen and nitrogen fragments. We can also plot energy-loss (ion chamber) versus TKE to identify elements, shown in Fig. 3.3. Both methods were combined to make a clean nitrogen gate.

There were 6556 events of Oxygen and 1961 events of Nitrogen in the data. Adding neutron time-of-flight gate (see Sec. 3.4) brought the total number of fragment-neutron coincidence events to 4758 of oxygen and 1120 of nitrogen.

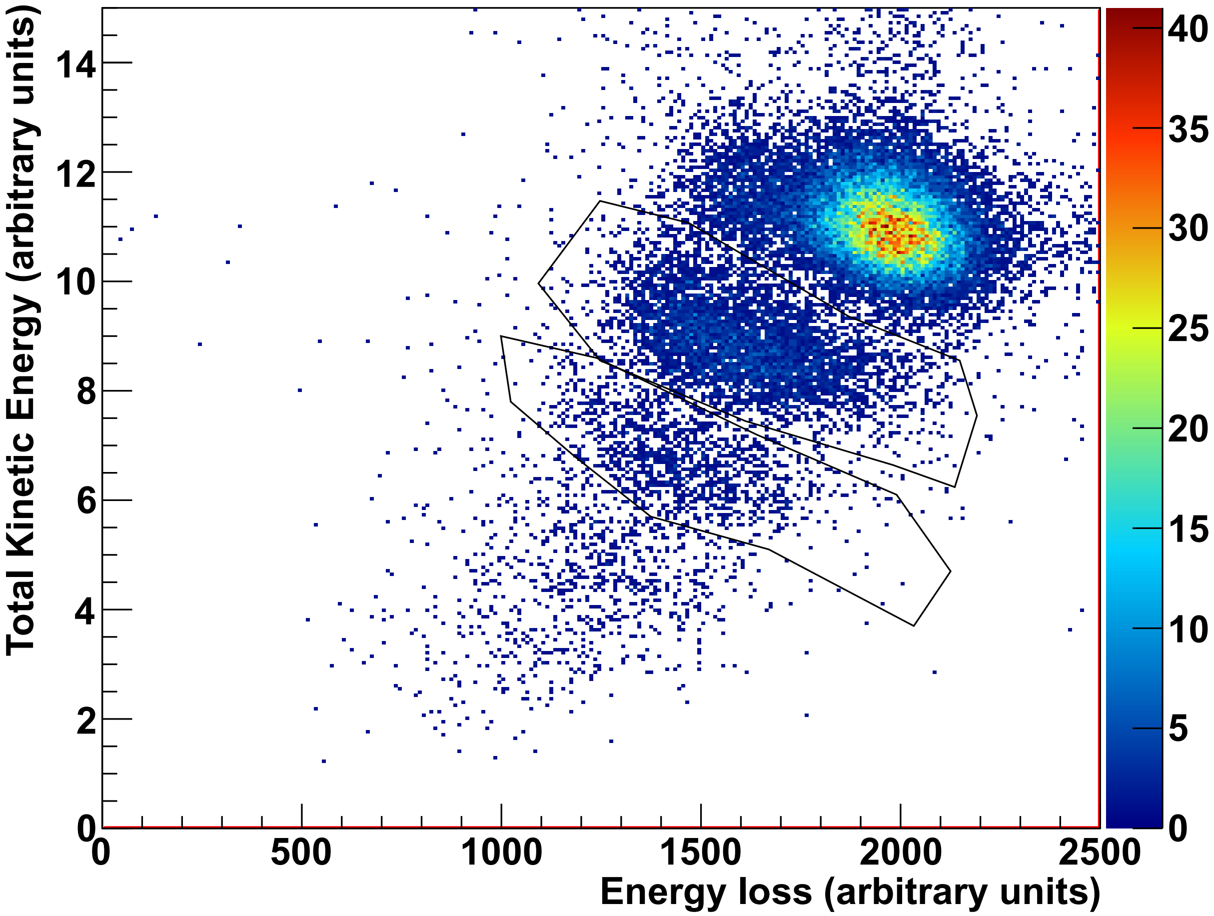

Figure 3.3: Element identification gated on incoming ^{26}F via energy loss versus total kinetic energy.

3.3 Isotopic Selection

Isotopic selection is traditionally achieved by separating the fragments of nitrogen by time-of-flight. However, since the flight paths through the Sweeper magnet are not uniform, mass selection directly from time-of-flight is not possible. As Fig. 3.5 illustrates, because the different isotopes have a different mass to charge ratios (A/Q) the direction of the flight paths exiting the sweeper are correlated with fragment mass. Therefore, we can introduce first and second order corrections for angle, position, and other parameters to correct the

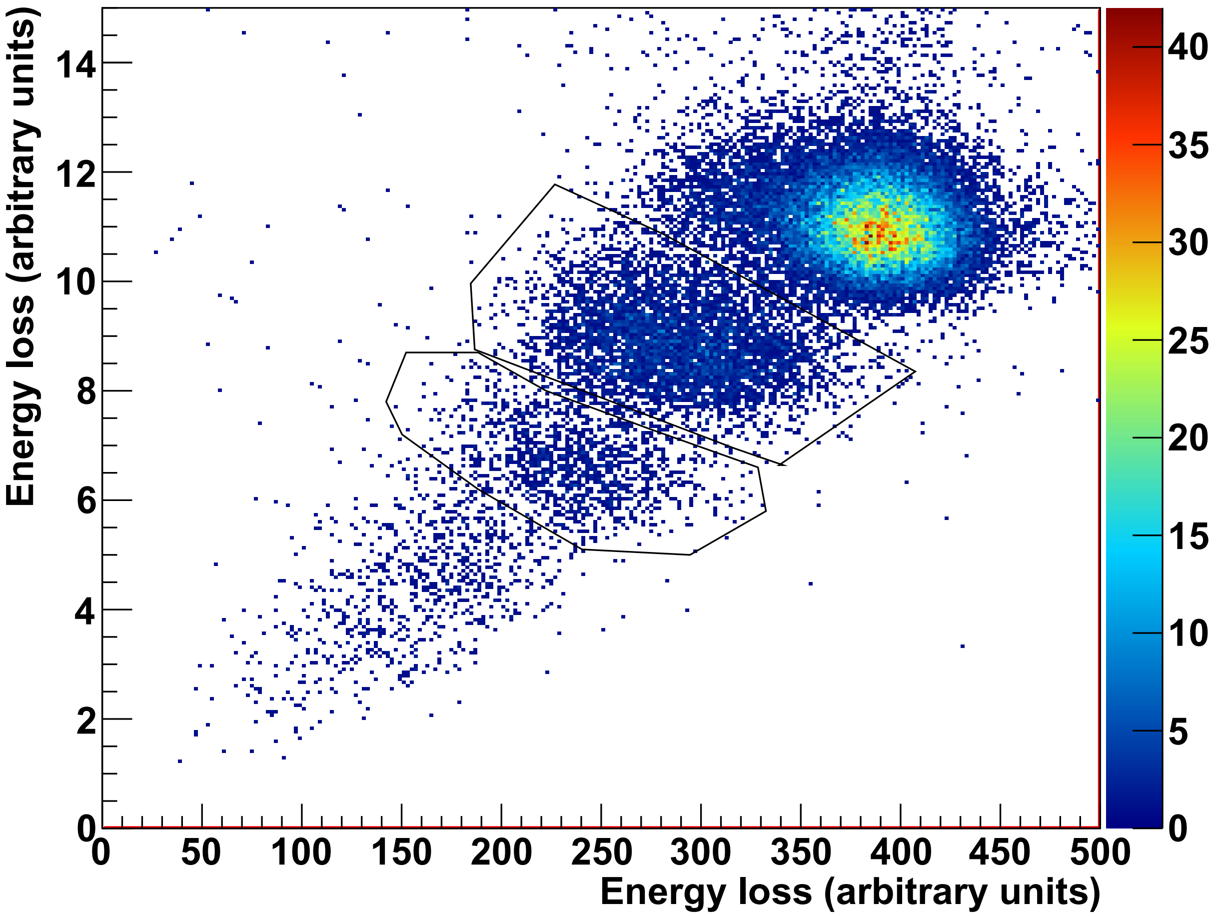

Figure 3.4: Element identification gated on incoming ^{26}F via energy loss versus energy loss (two different detector measurements).

time-of-flight. Dr. Hoffman found corrections that allowed separation of the oxygen isotopes, shown in Table 3.3. As shown in Fig. 3.8, the different isotopes of oxygen are correlated with angle. Because higher mass fragments of the same charge are deflected less than their lower mass counterparts, we know that higher mass is correlated with larger angle. Because ^{25}O is unbound and the sweeper was selected to let A/Q fragments of 3/1 through the center of the focal plane, the slowest isotope isotope in Fig. 3.6 is identified as ^{24}O.

Consider a similar plot for the nitrogen isotopes in Fig. 3.9. The same 3/1 ratio applies,

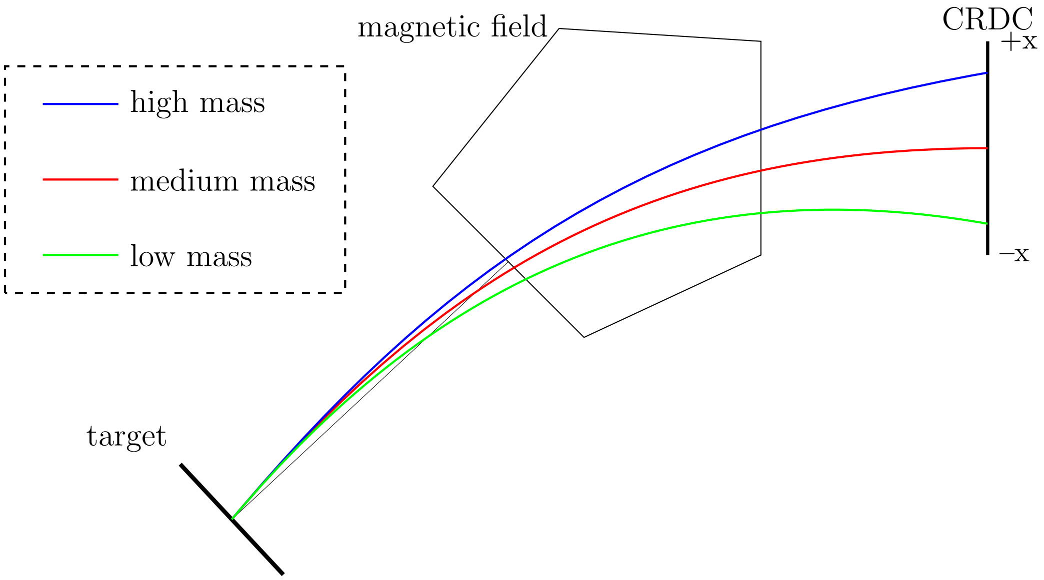

Figure 3.5: A diagram showing how isotope separation works. Beam fragments leave the target position with the same energy. Heavier isotopes (blue) are bent less than the sweeper magnet and thus end up with a positive angle and position in the focal plane. Lighter isotopes (green) and bent more by the sweeper magnet and thus end up with negative angles and positions at the focal plane.

Parameter	Coefficient	Description
Afp	60	1st order dispersive angle
Afp^2	-0.25	2nd order dispersive angle
Xfp	-3.5	1st order dispersive position
Xfp^2	-0.6	2nd order dispersive position
Xta	40	1st order target x position
Yta	20	1st order target y position
D_{flight}	0.25	flight path in focal plane

Table 3.2: Table listing the parameters of the corrected time-of-flight from Ref. [12]

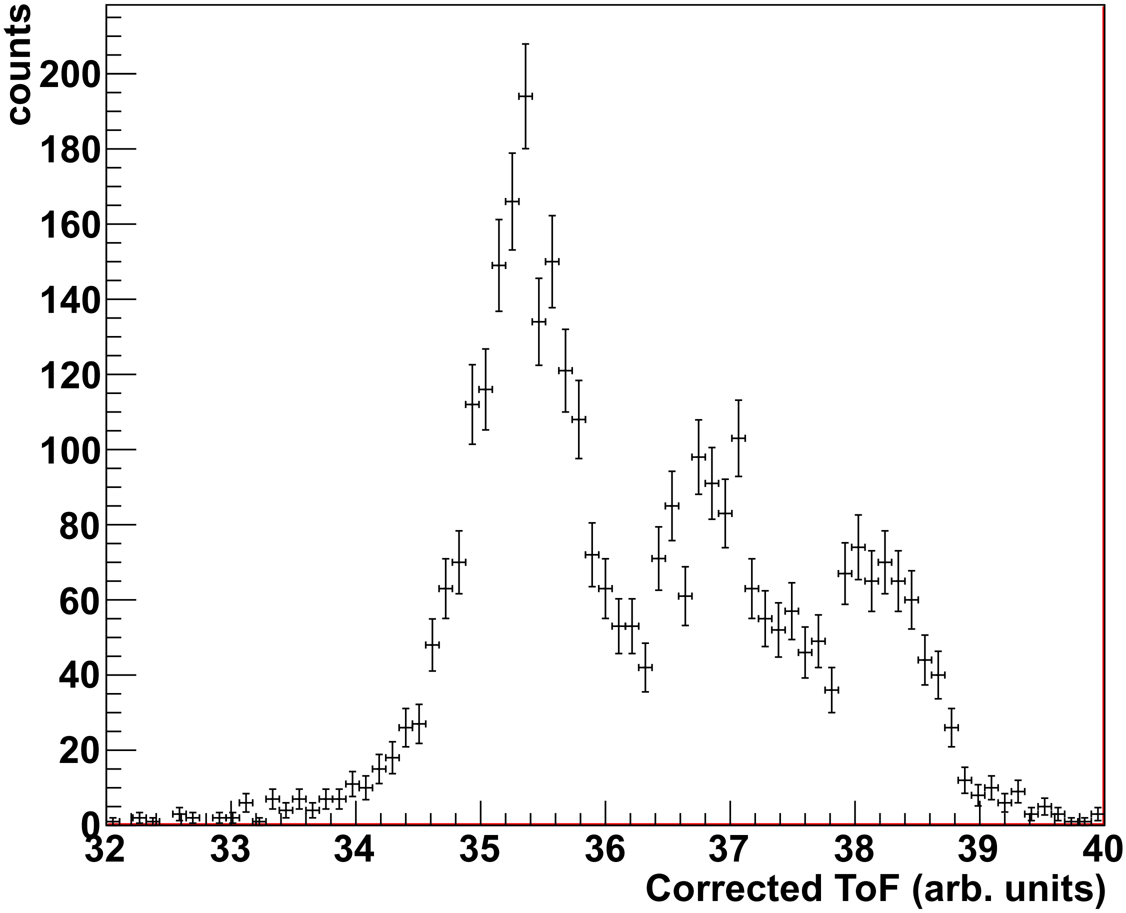

Figure 3.6: A corrected time-of-flight spectrum of oxygen fragments. The peaks correspond to individually separated isotopes (from shortest time-of-flight to longest) of ^{22}O, ^{23}O, and ^{24}O.

so the heaviest isotope, which is centered in the focal plane, is identified as ^{21}N (which has an A/Q ratio of 3/1). The subsequent lighter isotopes are ^{20}N and ^{19}N, which are clearly separated by the corrected time-of-flight in Fig. 3.7.

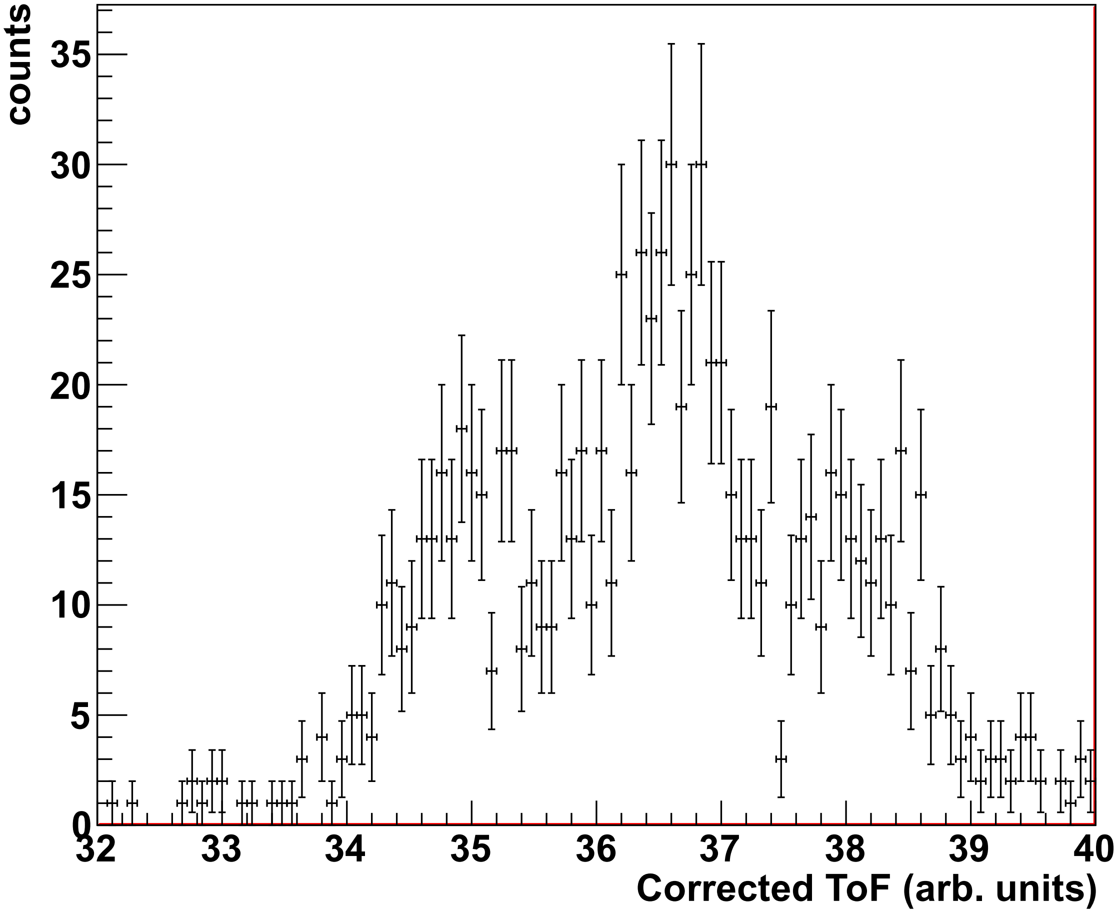

Figure 3.7: A corrected time-of-flight spectrum of nitrogen isotopes. The peaks lie in the same time of flight of the oxygen isotopes identified in Fig. 3.6, so the peaks from left to right are identified as ^{19}N, ^{20}N, and ^{21}N respectively.

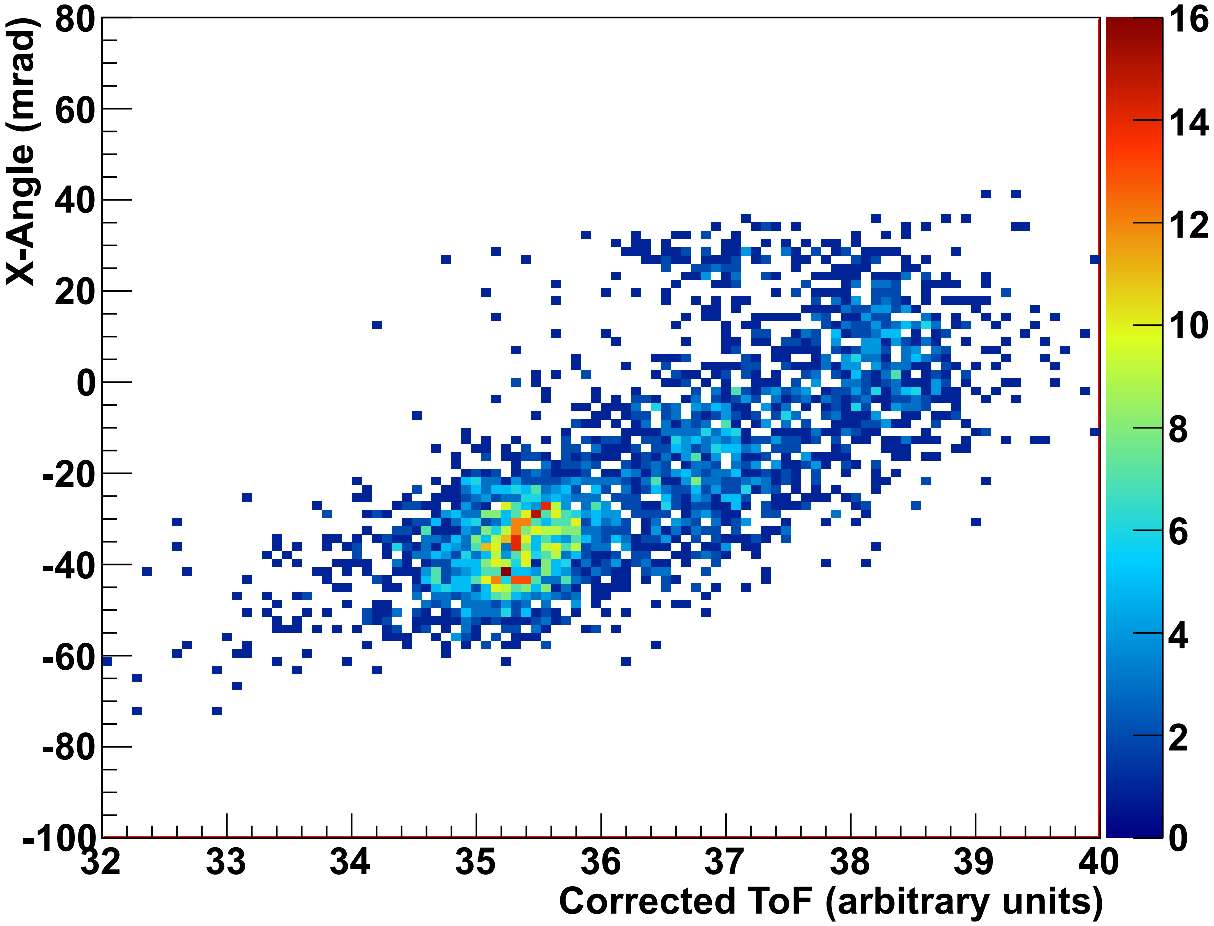

Figure 3.8: The angular correlation of oxygen isotopes to time-of-flight. The lighter isotopes are bent more by the sweeper magnet, so the isotopes of oxygen are identified (from left to right) as ^{22}O, ^{23}O, and ^{24}O.

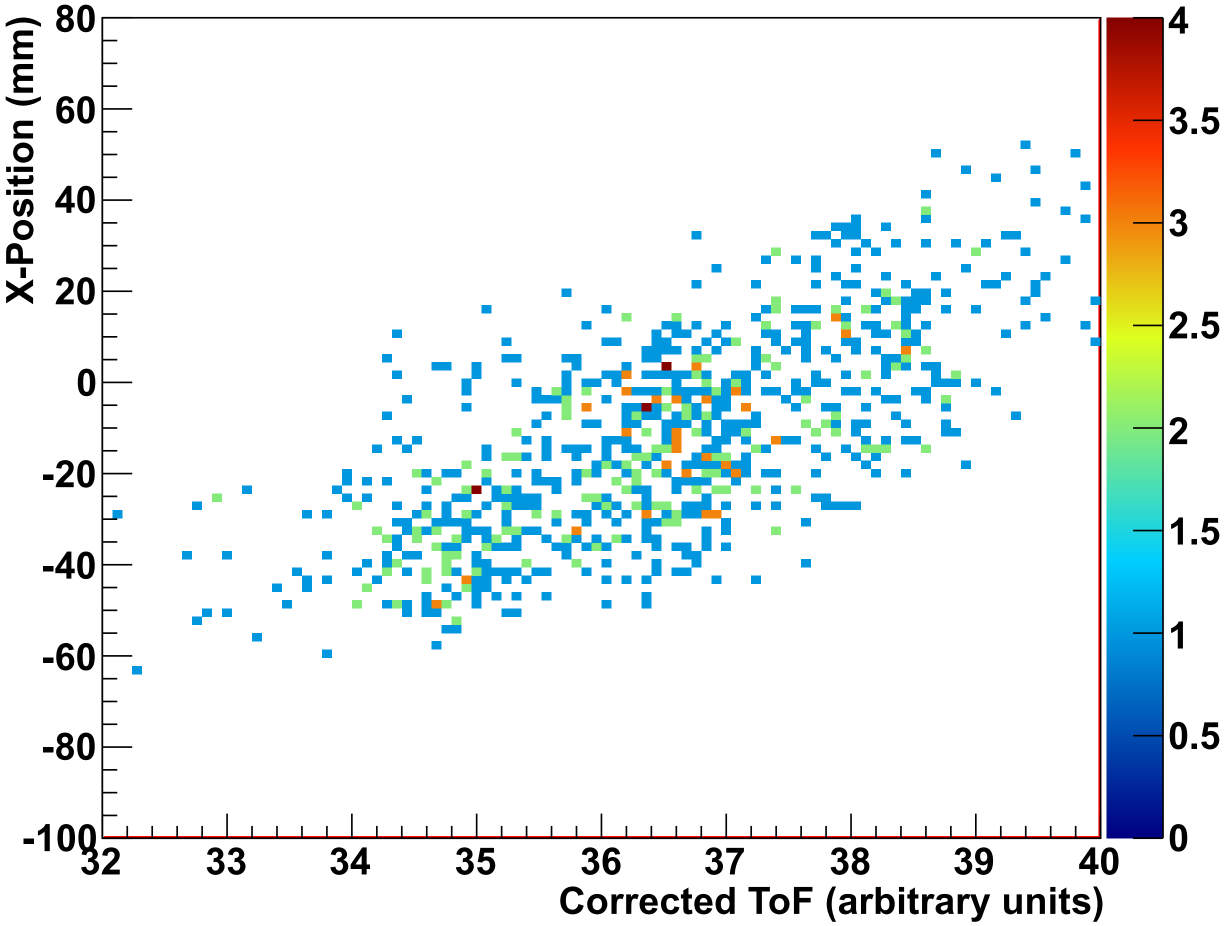

Figure 3.9: The angular correlation of nitrogen isotopes to time-of-flight. The lighter isotopes are bent more by the sweeper magnet, so the isotopes of oxygen are identified (from left to right) as ^{19}N, ^{20}N, and ^{21}N.

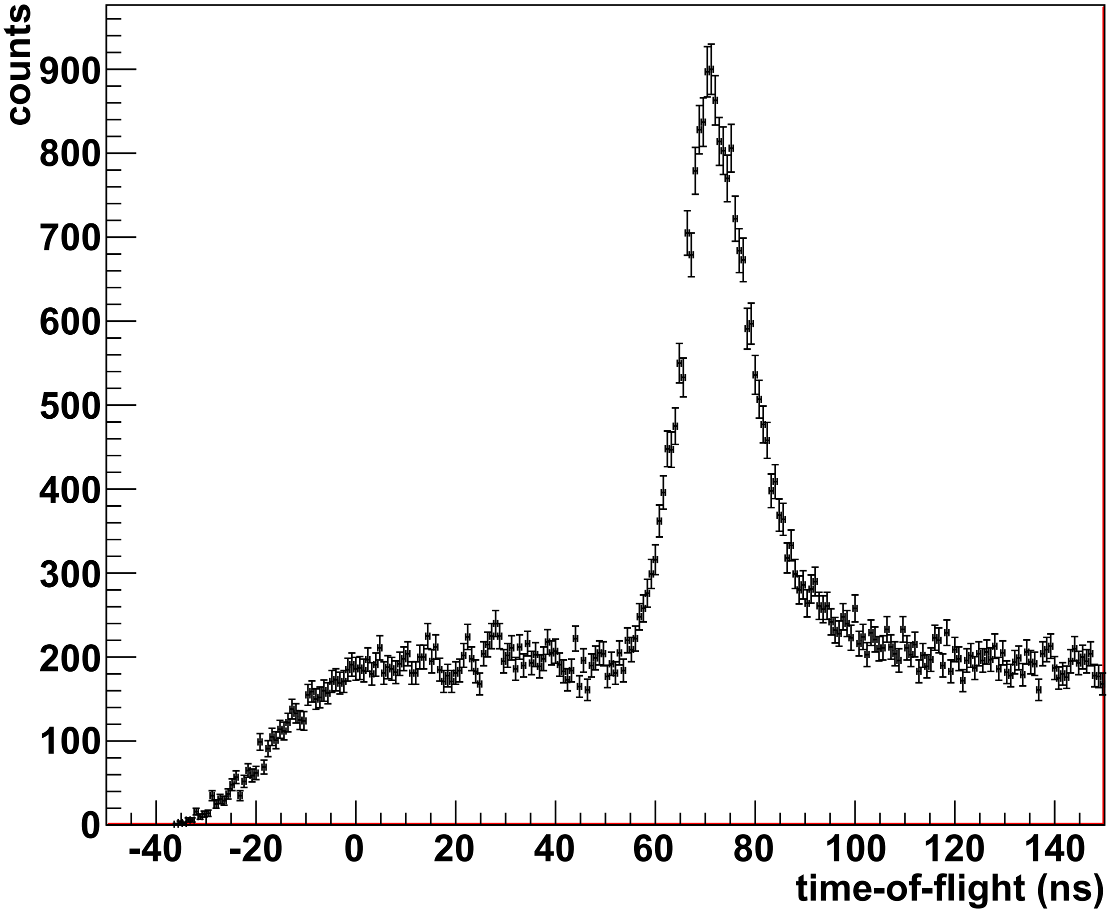

Figure 3.10: The total neutron time-of-flight spectrum. The peak at 68 ns corresponds to prompt neutrons from reactions on top of random background.

3.4 Neutron Coincidences

After identifying events that contain the isotope of interest, it is necessary to tag events that are coincident with a neutron. MoNA (the Modular Neutron array) is designed specifically to detect fast neutrons and the total neutron time-of-flight spectrum from MoNA is shown in Fig. 3.10.

Figure 3.11 shows the progression of adding more restrictive fragment gates to the total neutron time-of-flight spectrum. As fragment and isotope gates are added, the neutrons left are those that have the time-of-flight expected of decay neutrons at the same velocity as the beam. The expected time-of-flight is 68 ns, because that is the time it takes for 85 MeV/u neutrons to traverse 8.2 m.

3.5 Decay reconstruction

Invariant mass spectroscopy was used to reconstruct the decay energy (E_{decay}). Equation 3.1 shows the formula used for calculating the decay energy.

$$E_{decay} = \sqrt{m_f^2 + m_n^2 + 2(E_f * E_n - p_f * p_n * \cos(\theta_{open}))} - m_f - m_n \tag{3.1}$$

The equation takes into account the masses, energies, and momenta of the neutrons and the fragments as well as the opening angle between the two particles. The masses are taken from the most up-to-date atomic mass tables [1], while the rest of the parameters are measured observables.

For the neutrons, the angle is calculated from the interaction point in MoNA and the

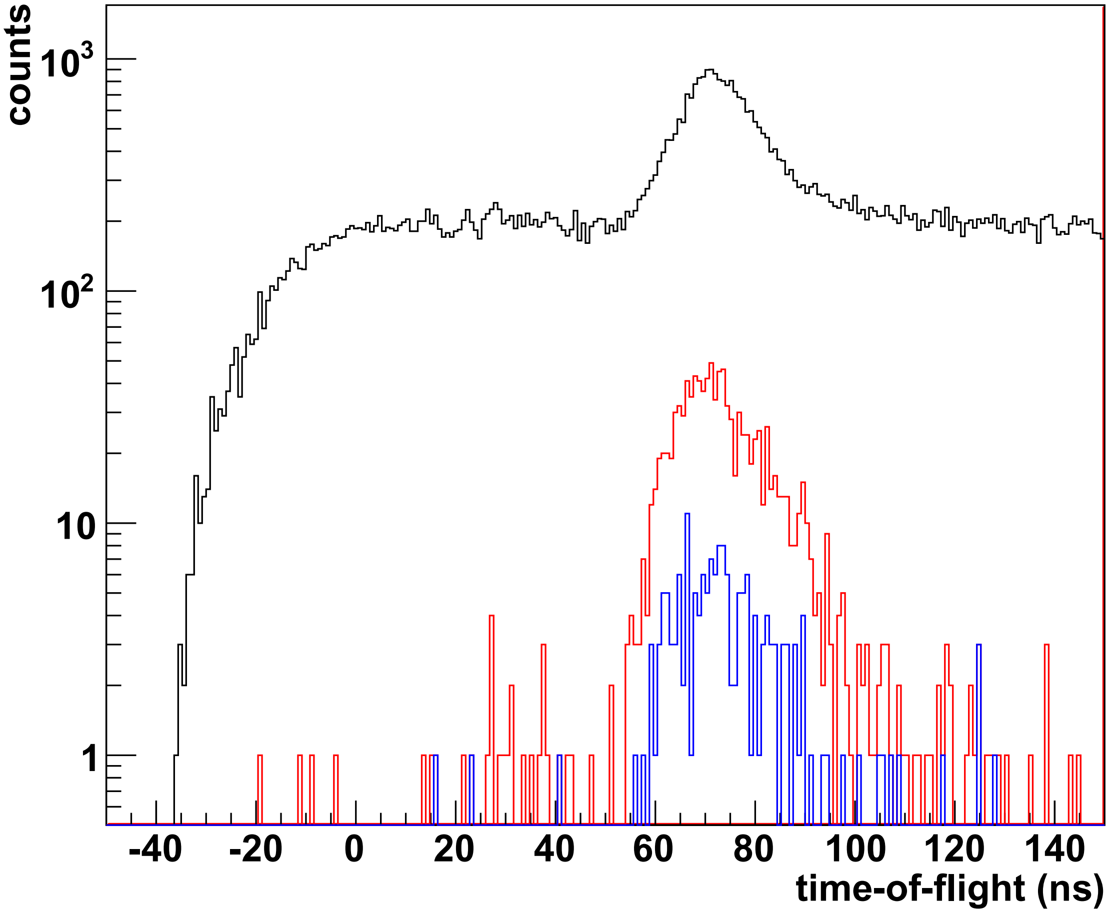

Figure 3.11: The progression of neutron coincidences as more restrictive element and isotope gates are applied. The black (top) spectrum is the total neutron spectrum from 3.10. The red (middle) spectrum is gated on nitrogen events, and the blue (bottom) spectrum is gated on ^{21}N events. This progression shows that the neutrons accompanying ^{21}N are likely to be "decay" neutrons from the break-up of ^{22}N.

energy and momentum is calculated from the time-of-flight and flight distance. For the charged fragments, the angles are reconstructed from a partial inverse matrix produced using COSY INFINITY [18], which also calculates the energy and momenta.

3.6 Monte-Carlo Simulations

In order to extract the energy of the resonance observed, Monte-Carlo simulations were performed. The software package ST-mona is designed to take into account the experimental resolutions and acceptances of the MoNA-Sweeper set-up in a Monte-Carlo simulation. These decay events are analyzed in the same manner as experimental events so they can be directly compared to experiment. Details of the simulation are given in Ref. [25, 23, 10, 12]. The geometrical acceptances and resolutions were taken from Ref. [12].

The ST-mona simulation procedure is as follows: experimentally determined input parameters of the secondary beam on target were used to calculate the positions and angles of the 2p-2n removal reaction inside the target. After the 2p-2n removal, the decay of the parent nucleus into a fragment plus the neutron is nearly instantaneous. Two different distributions were used for this analysis; a single symmetric Breit-Wigner for the resonance and a Maxwellian distribution for the non-resonance contribution.

After the decay the fragments are forward tracked through the Sweeper magnet using a forward ion-optical matrix created by COSY [18]. Neutrons are forward tracked to the position of MoNA. This allows for both neutron and fragment data to be directly compared to experimental data. Ref. [12] describes and shows how the experimental data matched the simulation for ^{24}O + n and ^{23}O + n events.

Since the simulation is produced in the same manner as the experimental data, the same invariant mass method can be used to make decay spectra that can be compared directly to data. The simulated decay spectra are fit to the experimental decay spectra to extract physical properties of the decay. This was carried out by varying the parameters of the distributions and adopting a goodness-of-fit minimum chi-squared (χ^2) value.

A single Breit-Wigner was used as the input for the resonance contribution of the decay while a Maxwellian distribution was used for the non-resonance contribution. The choice of a Maxwellian was an arbitrary choice because the low statistics do not justify extracting any physics from the non-resonant distribution. In fact, even the choice of the energy was arbitrary because the shape of the background was insensitive to the fit of the simulation to data.

The input for a Maxwellian distribution is:

$$f_E = 2\sqrt{\frac{E}{\pi kT^3}} \exp -\frac{E}{kT}$$

The free parameter of the distribution for fitting is kT, usually measured in MeV.

The basic equation for a resonance comes from Breit Wigner as shown in equation 3.2.

$$f_E = \frac{\Gamma}{(E - E_r)^2 + \frac{\Gamma^2}{4}} \tag{3.2}$$

Two physics parameters are extracted; the energy of the resonance (E_r in the equation) and the width of the resonance (Γ in the equation).

It should be noted that for these kinds of experiments with MoNA-sweeper, the actual width of the resonance in the decay spectrum is dominated by the resolution of the setup as shown in Fig. 3.12. The Breit-Wigner function plotted has a width of 6 keV while the input

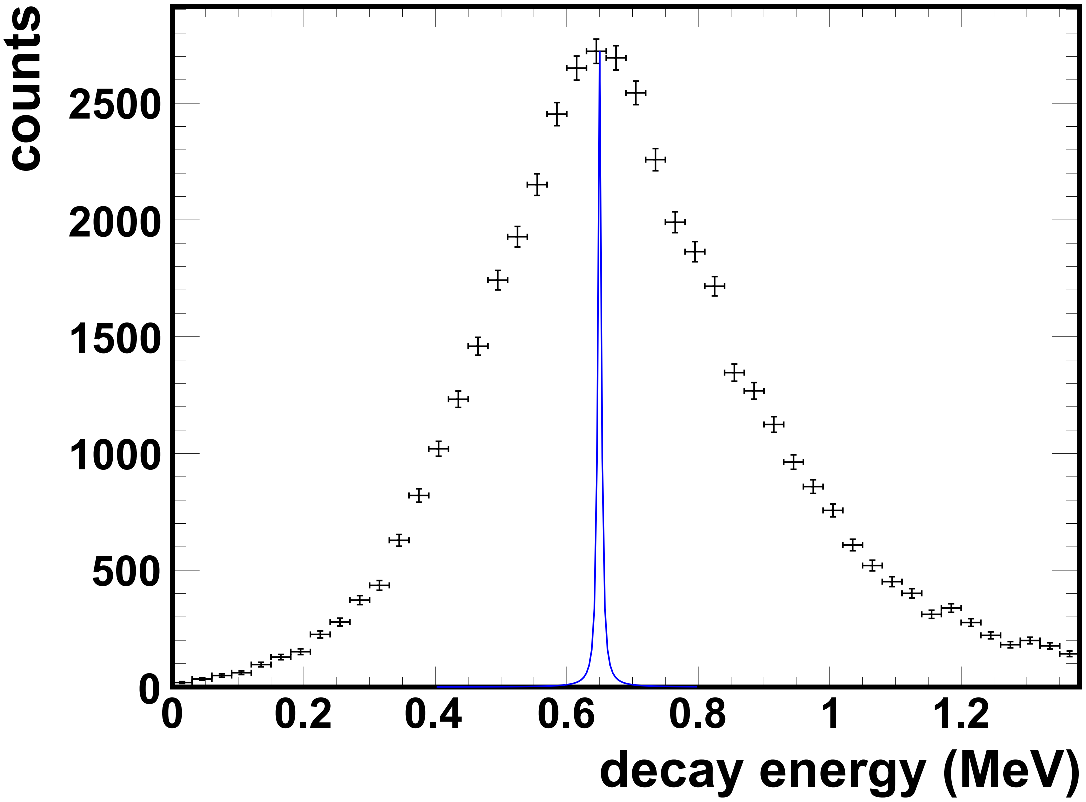

Figure 3.12: The data points indicate a narrow width Breit-Wgner resonance from a ST-mona simulation and the solid blue curve indicates the same Breit-Wigner resonance without any acceptances. The width of the decays were 6 keV with a energy of 650 keV.

of the simulation was a Breit-Wigner of zero width.

3.6.1 Fitting to data

Simulations with the resonance and the non-resonance decays were fitted via a minimization of χ^2 allowing the amplitudes of the contributions to vary freely as well as the energy and width of the resonance. The temperature of the thermal was insensitive to the fit, so an arbitrary choice of 6.5 MeV was taken to reduce the number of free parameters. A χ^2 fit of a Breit-Wigner resonance on top of a Maxwellian background yielded a decay energy of

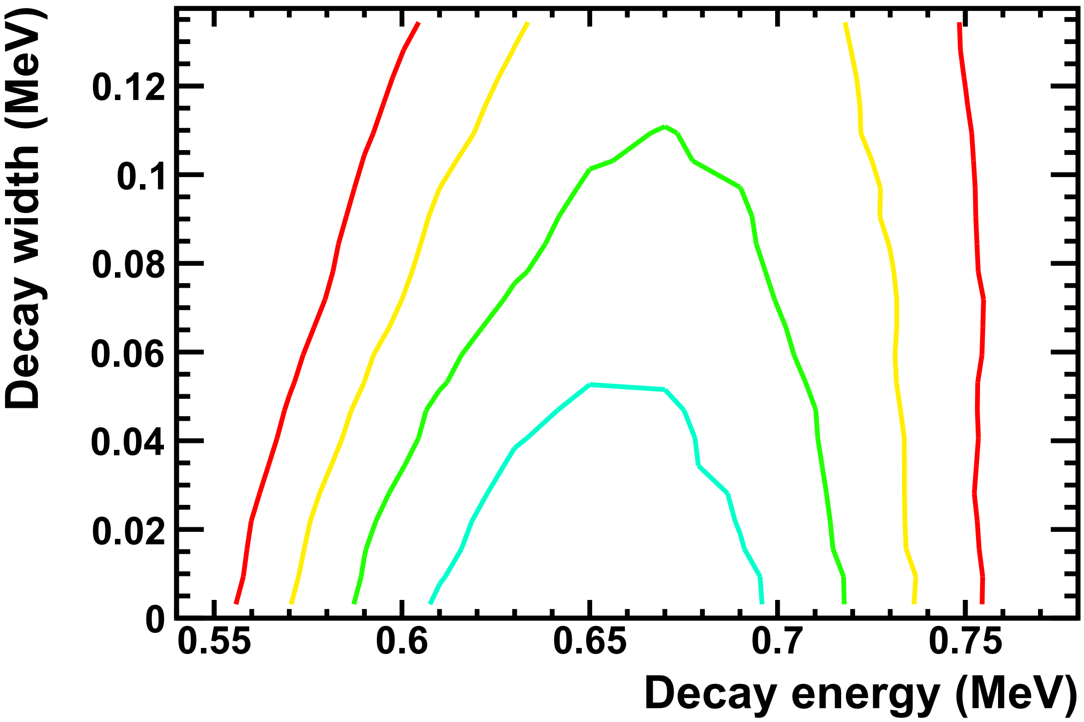

Figure 3.13: A contour plot of the χ^2 dependence of the Breit-Wigner parameters for the measured decay energy of ^{21}N + n. The parameters are the decay energy (x-axis) and the width of the decay (y-axis) in MeV. The lowest χ^2 is located at 0.65 MeV and 0 keV.

650 keV ± 50 keV with zero width. Figure 3.13 shows the 1-σ and 2-σ confidence levels of the fits. The width of the resonance was dominated by the experimental resolution of the experimental set-up and only an upper limit of 60 keV could be established from a 1-σ limit.

Figure 3.14 shows the final fit to the data.

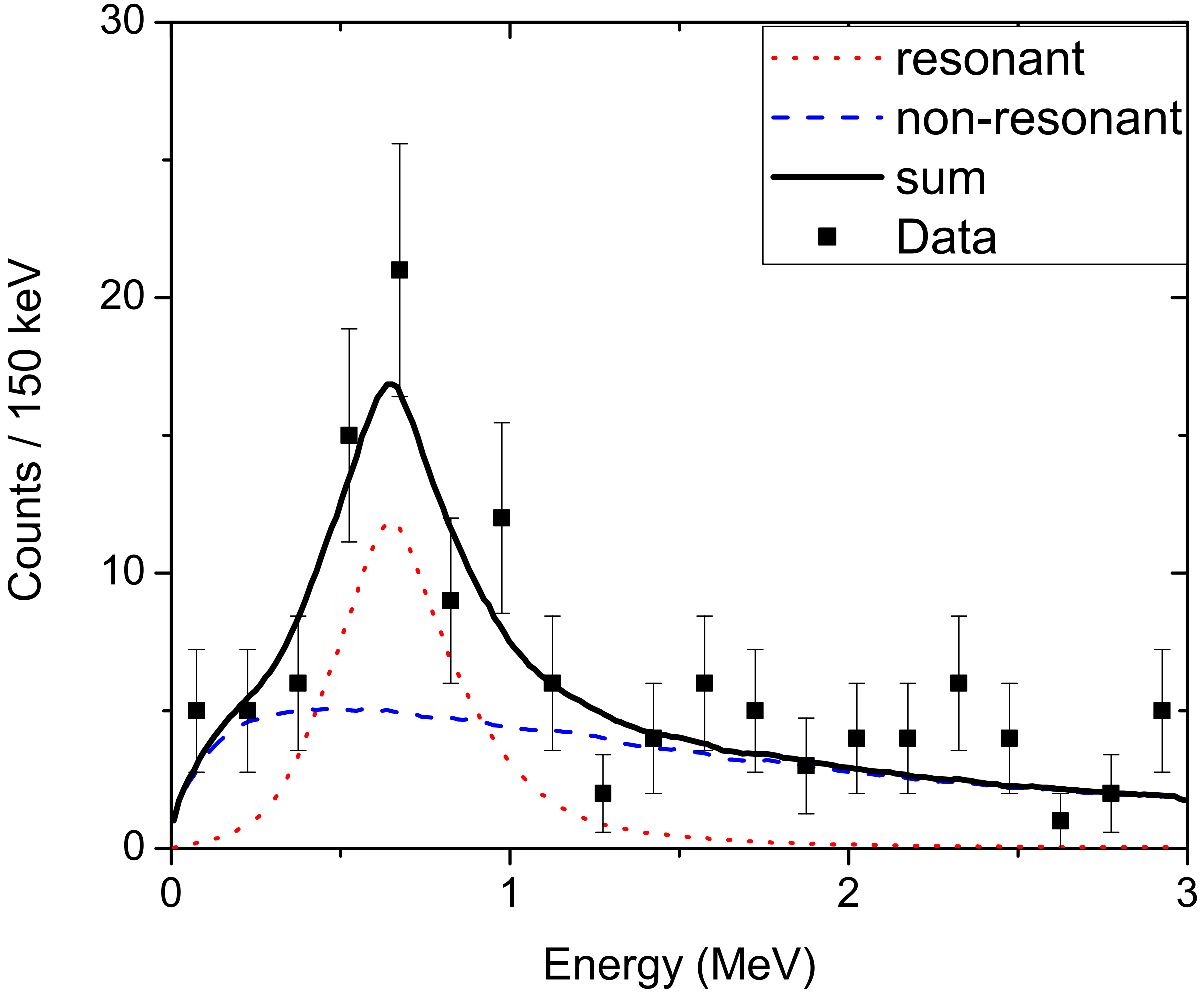

Figure 3.14: Neutron-decay energy spectrum of ^{22}N. The data with statistical error bars were measured by requiring a coincidence between an identified ^{21}N fragment and a neutron. The solid line is the sum of the resonant (dotted) and non-resonant (dashed) contributions of a Monte-Carlo simulation that takes into account the resolutions and acceptances of the experimental apparatus. The resonance line-shape is a Breit-Wigner with $E_{\mathrm{decay}} = 0.65(5)$ MeV.

Chapter 4

Results and Discussion

In order to extract the excitation energy of the resonance observed, the binding energy has to be added to the decay energy. The neutron separation energy of ^{22}N is 1.28(21) MeV [1]. Adding this to the resonance of 0.65(5) MeV results in an excited state energy of 1.93(22) MeV. It is interesting to note that although the statistics for the determination of decay is rather limited, the uncertainty of the excitation energy is still dominated by the uncertainty of the mass measurement.

The underlying assumption is that the observed decay goes to the ground state of ^{21}N. While we cannot rule out the possibility that the resonance decays to an excited state of ^{21}N, an examination of the level scheme in Fig. 4.1 shows that this case is unlikely. The lowest measured excited state of ^{21}N (a $3/2^-$ state) is located at 1.177 MeV [27], which would place the resonance above 3 MeV in ^{22}N. This is unlikely, because none of the commonly used shell model interactions predict the first unbound excited state of ^{22}N at such a high excitation energy.

The spin and parity assignment of the observed resonance is guided by shell model cal-

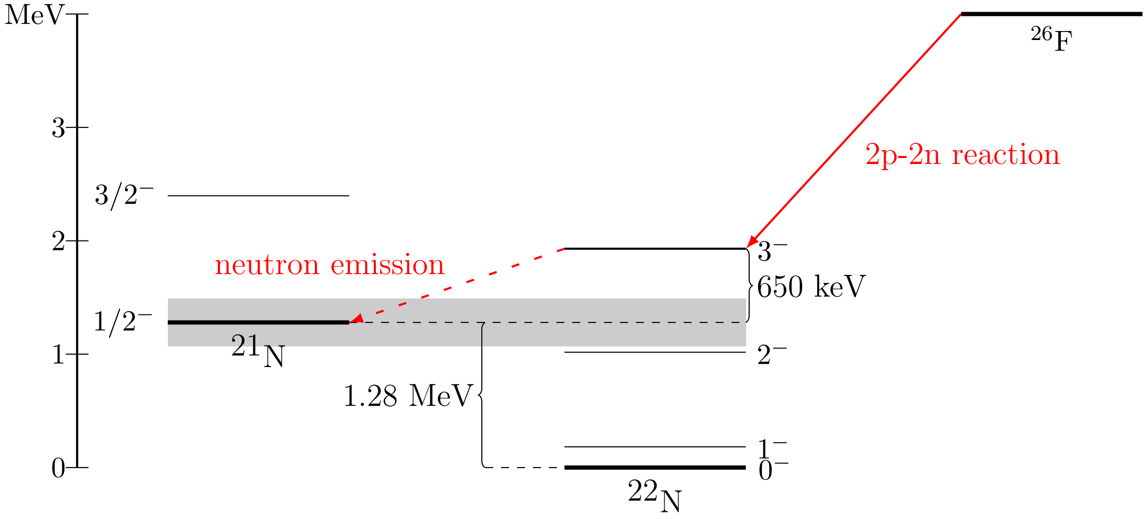

Figure 4.1: The proposed level scheme of ^{22}N → ^{21}N + n decay created from a reaction of ^{26}F.

culations. This is the common approach to analyze states in nuclei far from stability where angular distribution measurements are difficult. The ground state of ^{22}N has been assigned a spin and parity of 0^-. Sohler *et al.* [27] identified the first two excited states of ^{22}N to be 1^- and 2^- respectively, guided the shell model. The next predicted state is a 3^-, thus we attributed the decay observed to be the 3^-.

B. A. Brown [5] calculated the single particle width for a $0d_{5/2}$-wave decay at 650 keV to be 55 keV. With the spectroscopic factor for a 3^- to $1/2^-$ decay equal to 0.1059 (calculated via the shell model [7]), the observed width would be 5.8 keV which is within the upper limit of the width observed at 60 keV.

The second 2^- state of ^{22}N, which would decay in a $0d_{3/2}$-wave decay is unlikely to be the state observed by this experiment because the expected width of such a state ($\sim$ 500 keV [5]) is an order of magnitude larger than the maximum possible width observed. Also, since we populate this state from a beam of ^{26}F, there is only one neutron in the $\nu 0d_{3/2}$ shell, as shown in Fig. 4.2. Since this is the outermost shell, the cross section to strip out this nucleon

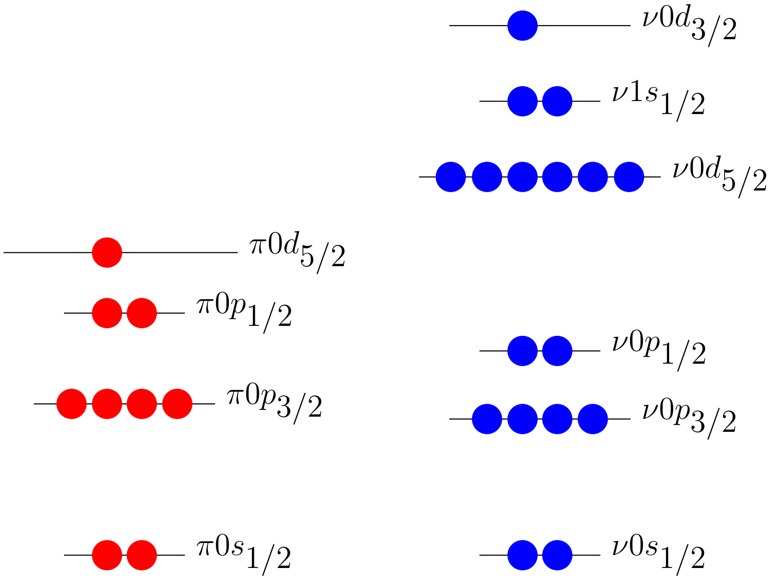

Figure 4.2: The ground state shell configuration of ^{26}F. Note the lone neutron in the $\nu 0d_{3/2}$ shell.

in a multiple nucleon stripping reaction is quite high.

4.1 Shell model calculations

Shell model calculations using the code NuShell@MSU [7] were carried out for ^{22}N levels. Because the USD TMBE used in the WBT interaction reproduce the level energies for oxygen isotopes successfully, but not the carbon isotopes, Staniou *et al.* [30] proposed a 25% reduction of the neutron-neutron TBME to make a better empirical agreement for the neutron rich isotopes of carbon. Sohler *et al.* [27] observed the same compression for nitrogen isotopes and thus a 12.5% reduction (half of 25%) was proposed. These reductions were justified by comparing the calculation to measured bound excited states of several neutron rich nitrogen ($^{19-22}$N) and carbon ($^{17-20}$C). We reproduced these calculations with the code NuShell@MSU. We applied the same 12.5% reduction to the WBT and WBP interactions (called WBTM and WBPM respectively).

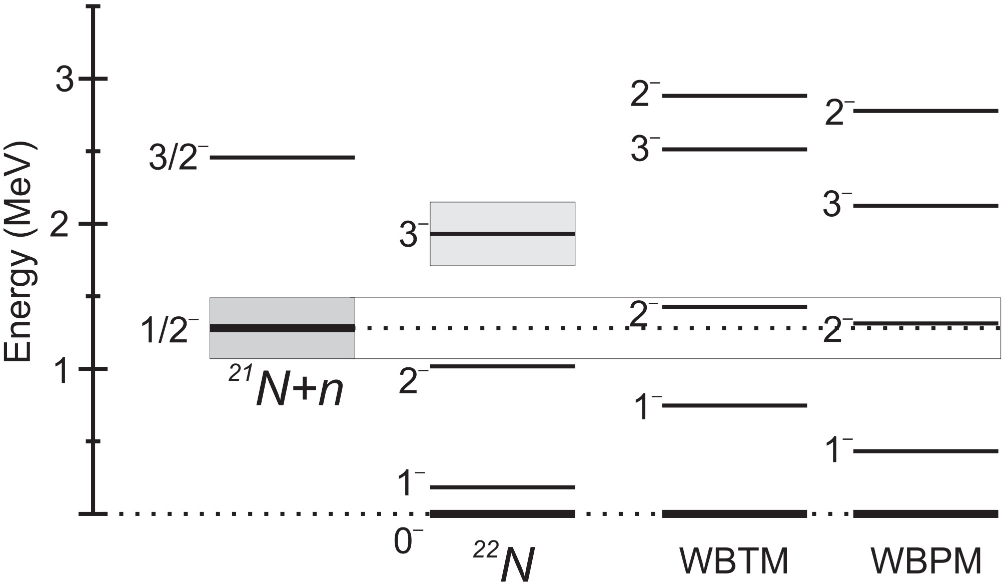

Figure 4.3: Level scheme of ^{22}N. The present experimental data are shown together with the data of Reference [27] and are compared to WBTM and WBPM shell model calculations. The neutron separation energy as well as the ground and first excited state of ^{21}N are also shown. The shaded area around the ^{21}N ground state represents the uncertainty due to the neutron separation energy. The shaded area around the measured 3^- state corresponds to the excitation energy uncertainty which is dominated by the uncertainty of the neutron separation energy.

Figure 4.3 shows the results of NuShell calculations for ^{22}N excited states. As can be seen, the calculated levels with the WBTM are consistently at higher excitation energies compared to measured levels, especially the 1- state. Calculations using the WBP Hamiltonian, which uses a different choice in the fitting of *psd* levels, showed an improvement in energy for the 1^- state. We applied the same 12.5% decrease of the neutron-neutron interaction strength to the WBP interaction (label as WBPM interaction in Fig. 4.3) which resulted in an improved overall agreement with the data. The excitation energy of the 3^- calculated with the WBPM interaction is 2.12 MeV which is within the uncertainty of the measured resonance. It should be noted that the modified theoretical calculation of the 2^- state shows that it is within the uncertainty of the neutron separation energy of ^{22}N.

Another way to look at what would be predicted for the 3^- state of ^{22}N is to examine the measured results for ^{20}N. The first two states for ^{20}N are a $(\pi 0p_{1/2})\times(\nu 0d_{5/2})$ configuration, so by the triangle condition the spin-parity is 2^- or 3^-. The ground state is 2^- and the first excited state is 3^-. The shell model was successful in predicting the energy of the excited state energy of ^{20}N. Now the ^{22}N has the same configuration as ^{20}N with the exception being a filled $\nu 1s_{1/2}$ shell. So the energy difference between the 2^- and 3^- in ^{22}N should be similar to the 2^- and 3^- in ^{20}N. Adding in the excited energy of ^{20}N to the measured energy of the 2^- state of ^{22}N gains:

$$E_{2-} + E_{3-} = 1.09 + 1.02 = 2.11 \text{ MeV} \tag{4.1}$$

This compares favorably with our measured 3^- energy of 1.93(23) MeV.

4.2 Disappearance of the N = 14 shell

As described earlier in Sec. 1.4, performing a weighted average of states corresponding to particular shell orbits will yield a gap in energy between the shells. This allows experimentalists to predict and confirm a level inversion between two orbits. Shown in Fig 1.7, Talmi and Unna [31] used this method to confirm a level inversion between the $0s_{1/2}$ and $p_{1/2}$ shells in ^{11}Be. Similarly, Talmi and Unna [31] used averaging of states in the N = 9 isotones to predict a level inversion of the $\nu 0d_{5/2}$ and $\nu 1s_{1/2}$ shells. This result is confirmed in shell model calculations that show that the $\nu 1s_{1/2}$ goes down in energy as protons are removed from ^{17}O. Comparing the levels for $N = 9$ for oxygen (Fig. 1.4) and for carbon (Fig. 1.5) bears this conclusion out. As neutrons are added to the N = 9 isotopes the orbits return to their normal ordering because the $0d_{5/2}$ drops in energy as it is filled with neutrons.

We can take a similar approach in analyzing the $N = 14$ shell gap for the $N = 15$ isotones. The $N = 14$ shell gap is the gap in energy between the $\nu 1s_{1/2}$ and the $\nu 0d_{5/2}$ shells. The shell gap for ^{23}O is 2.79 MeV as evidenced by the measured excited state energy of the $5/2^+$ state [26]. (Only one excited state is necessary for ^{23}O because the $5/2^+$ is the only possible configuration as shown in Fig. 1.9). With the addition of the 3^- state of ^{22}N to the known states of ^{22}N, we can estimate the shell gap for ^{22}N. The $2J + 1$ summing average of the 0^- and 1^- states corresponds to the $\nu 1s_{1/2}$ level and the average of the 2^- and 3^- corresponds to the $\nu 0d_{5/2}$ level. The resulting gap of 1.41(17) MeV, significantly smaller than the $N = 14$ shell gap of 2.79(13) MeV deduced for ^{23}O. This reduction of 1.38(26) MeV in the $N = 15$ isotones is consistent with the reduction of 1 MeV reported between ^{22}O and ^{21}N for the $N = 14$ isotones [27]. The continuation of the reduction of the size of the shell gap and perhaps the emergence of the level inversion can be calculated using a linear extrapolation first introduced by Talmi and Unna [31]. Figure 4.2 shows the measured difference between the $\nu 1s_{1/2}$ and $\nu 0d_{5/2}$ levels for the $N = 15$ oxygen and nitrogen isotones with extrapolation to ^{21}C. The extrapolation suggests that the levels are essentially degenerate (0.03 MeV) in ^{21}C. Within the experimental uncertainty, the levels could be again inverted similar to the level inversion of ^{15}C.

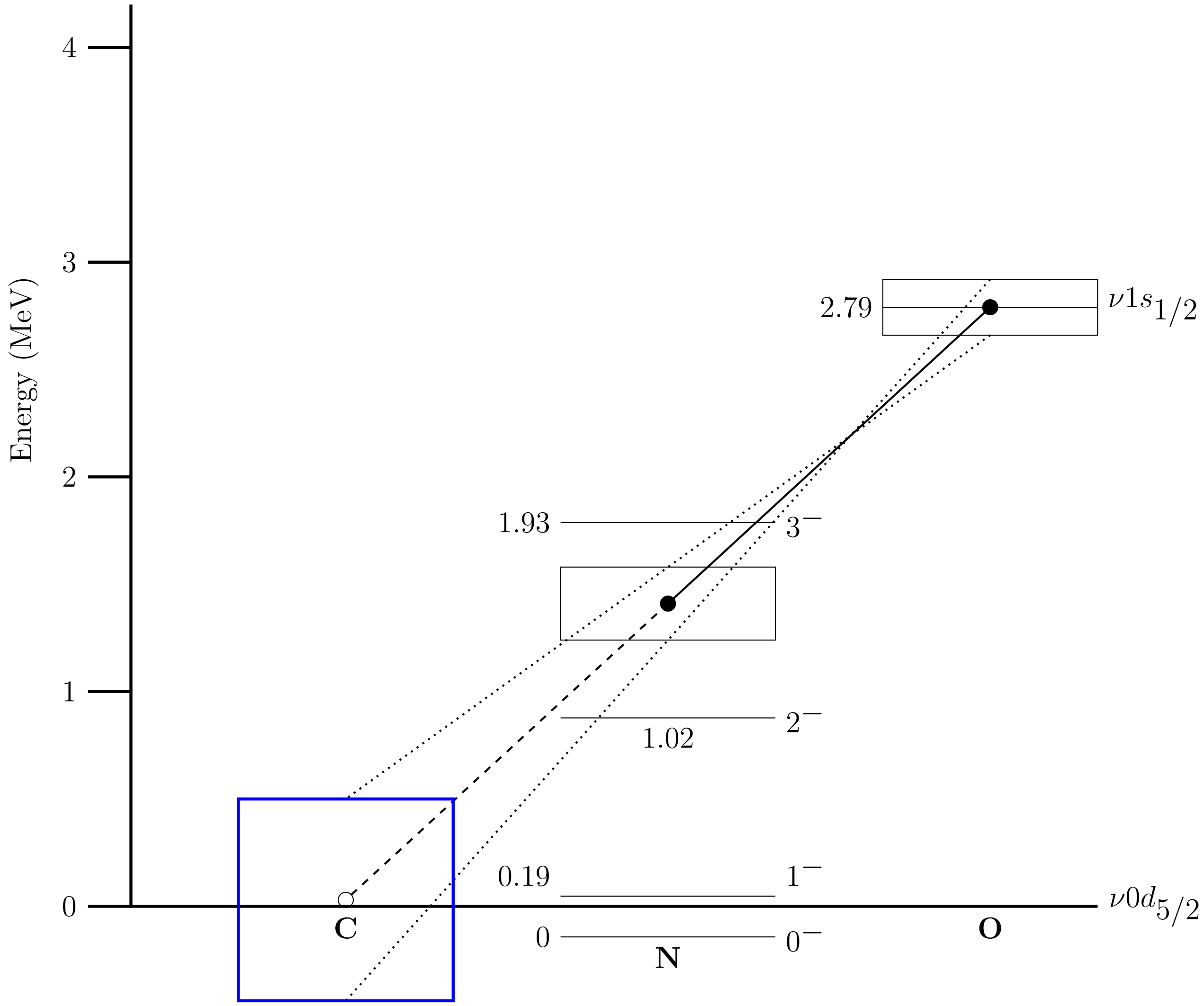

Figure 4.4: The "competition" between the $\nu 1s_{1/2}$ and $\nu 0d_{5/2}$ levels for the N = 15 isotones of carbon, nitrogen, and oxygen following the prescription of Ref. [31]. Experimental data for the levels of ^{23}O and ^{22}N are taken from Refs. [26],[30],[27], and this work. It should be noted that the states labeled $\nu 1s_{1/2}$ are actually $\nu 0d_{5/2}$-hole states, but these states measure the $\nu 1s_{1/2}$ level because a neutron is required to move from the $0d_{5/2}$ to the $1s_{1/2}$. The blue box around ^{21}C indicates the range of expected gaps for the ground state based on the error bars of the ^{22}N and ^{23}O measurements.

Chapter 5

Conclusion and Future prospectives

We report here the measurement of a resonance of 650(50) keV, from the neutron decay of an excited state in ^{22}N. This state was induced from reactions of a 85 MeV/u ^{26}F beam on a beryllium target. The decay fragments and neutrons were detected by the MoNA-Sweeper set-up and reconstructed to achieve a decay energy. We attributed this to the neutron decay of the first 3^- state of ^{22}N with an excitation energy of 1.93(22) MeV.

Combining this result with previous work on excited states of ^{22}N by Sohler *et. al.* [27], we calculated a $N = 14$ shell gap of 1.41(17) MeV for ^{22}N. Having established the $N = 14$ gap for the $N = 15$ nucleus ^{22}N from a weighted average of the $\nu 1s_{1/2}$-particle and $\nu 0d_{5/2}$-hole states of ^{22}N, we combined these results with previous measurements of the $N = 14$ shell gap for ^{23}O, ^{22}O and ^{21}N. Extrapolation of the energy between the $\nu 1s_{1/2}$ and $\nu 0d_{5/2}$ for the the $N = 15$ isotones point to a possible inversion in the orbitals for ^{21}C. This would be a similar effect to the one observed by Talmi and Unna [31] of the inversion of the $\nu 1s_{1/2}$ and $\nu 0d_{5/2}$ orbitals in the $N = 9$ isotones.

This extrapolation leads to the conclusion that the assignment of the angular momentum

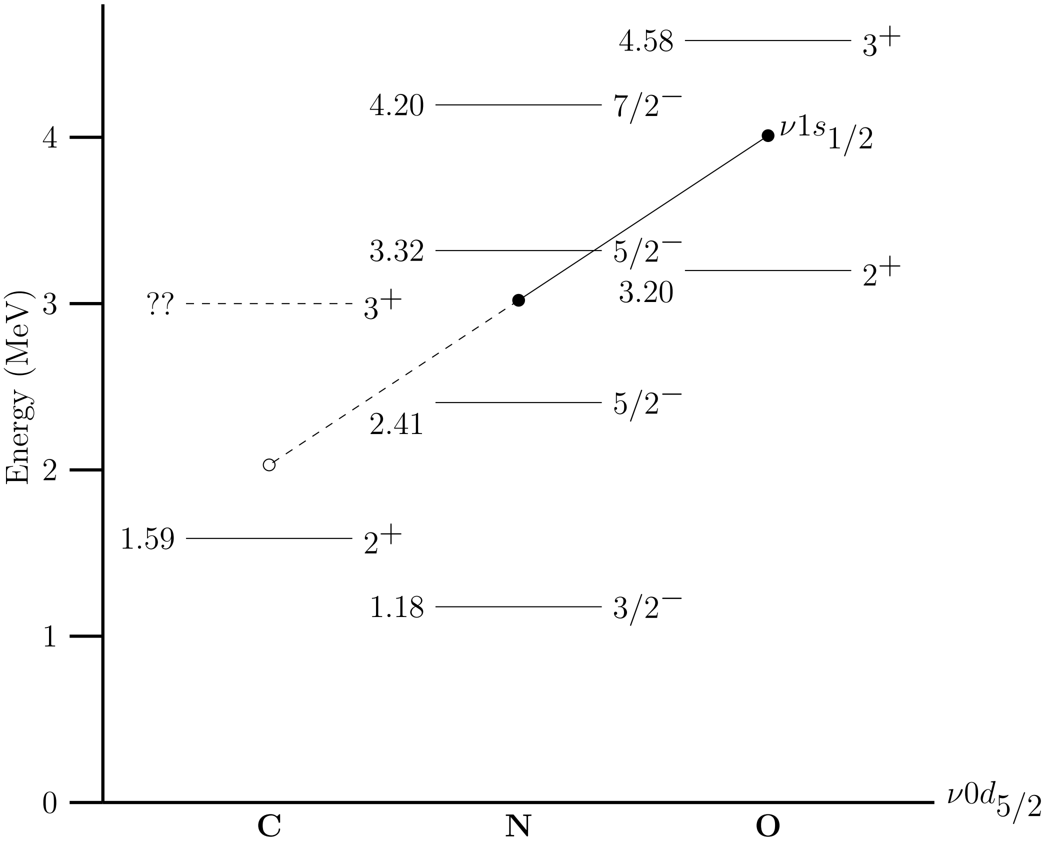

Figure 5.1: The "competition" between the $\nu 0d_{5/2}$ and $\nu 1s_{1/2}$ levels for the $N = 14$ isotones of carbon, nitrogen, and oxygen following the prescription of Ref. [31]. Experimental data for the levels of ^{22}O, ^{21}N, and ^{20}C are taken from Refs. [30],[29], and [27]. Higher excited states in ^{20}C, like the next expected $\nu 1s_{1/2}$-particle state with $J^{\pi} = 3^{+}$, have not been observed.

of the ground state ^{21}C may not be trivial. The possibility exists that the ^{21}C ground state is $5/2^{+}$ and not $1/2^{+}$ (the shell configuration is shown in Fig. 5.2). It would be interesting to measure the ground state energy of ^{21}C as well as investigate the J of ^{21}C.

There have also been incomplete studies of the N = 14 gap for the N = 14 nucleus ^{20}C. Fig. 5 shows the same analysis of $1s_{1/2}$-$0d_{5/2}$ gap for the $N = 14$ isotones. As the linear extrapolation suggests a reduction of the gap for N = 14 isotones, however, measurements for the N = 14 carbon isotope 20C is incomplete. Stanoiu *et. al.* [30] measured the excited states of carbon isotopes and found only one bound excited state for ^{20}C, a 2^{+} state at

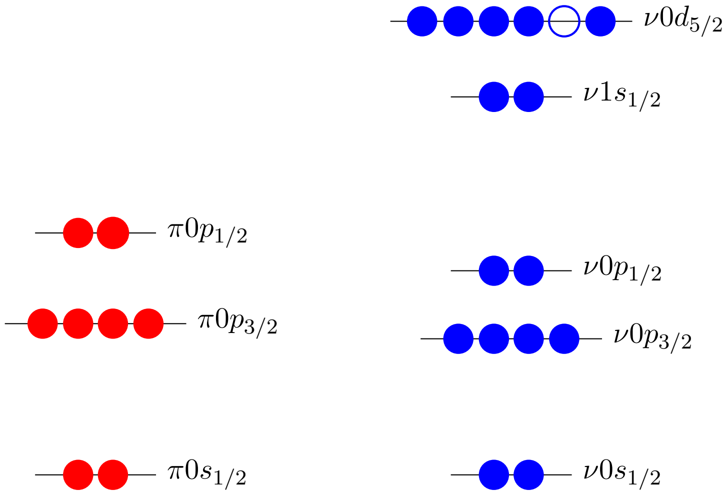

Figure 5.2: The shell configuration of an inverted ground state of ^{21}C.

1.588 MeV. Measuring the 3^+ excited state of ^{20}C would complete the levels needed to calculate the $N = 14$ shell gap. Since it was not observed in gamma spectroscopy, neutron decay spectroscopy is needed to measure this state.

While we have found the dripline up to neon, the neutron drip line above neon remains a mystery. With new experiments exploring the upper limits of stability, physicists have found isotopes that are bound more than we ever thought before. For example, a recent experiment at the NSCL discovered two neutron rich isotopes of ^{40}Mg and ^{42}Al [2] provide evidence that the dripline is further slanted to neutron rich nuclei than we have thought. The emergence of new magic numbers and closed shells is likely to continue.

Appendix A

New Experiment Setup Guide

A.1 Introduction

The purpose of this document is to describe how to create and manage a new MoNA-LISA-Sweeper experimental account. Most of the following procedures can be done from a data_U machine by logging in with the experiment user account.

While the original guides attempted to do a step by step procedures for everything, the adoption of ROOT for analysis (with its vast customizability and extensibility) has made such procedures moot because an experimenter might have different choices for online-analysis or daq needs. Every attempt will be taken to make this coherent and that newbies can read this guide, but the following rule applies: There is more than one way to skin a cat.

A.2 The Purpose of Experimental Accounts

The entire purpose of an experimental account is provide the following for the experimenter:

- Provide space to temporarily store data from the experiment in a write protected disk space, called event space.

- Provide a location for customized programs that run the experiment. Some examples include: the data acquisition, online data analysis, high voltage controls, and trigger logic.

There are four kinds of Linux computers that can access the experimental account. These are the data acquisition computers (DAQ), called spdaq-machines, the data_U machines, and the element (32-bit) and the fishtank (64-bit) machines. The spdaq and data_U machines have the same architecture, however, the spdaq machines (located in the vault) are dedicated for use in data acquisition. The data_U machines can access the spdaq machines (more on that later) and can be used to do special online analysis without taking up CPU of the spdaq machines. Both spdaq and data_U machines has access to the event space (`\events\`). While the element and fishtank machines have the same user area as the data_U and spdaq machines, they do not access to event space. They can be used for offline analysis after the data has been copied to evtdata space (a non-write protected disk space for data).

All the current codes and files for running a MoNA-LISA-Sweeper experiment are located in the `monasoft` account. They can be accessed and copied directly from the `/user/monasoft` account or via cvs [1].

A.3 Acquiring the Experimental Account

A couple weeks before the experiment is scheduled to run you should request the computer department to create a user account. The user account name is set to the experiment number

---

[1] cvs is a version control system used manage changes in code for important programs. It requires “checking out” code from a repository in the `monasoft` account.

(#####) issued by the PAC with an e in front (like e03038 or e05124). If several different accounts for the same experiment are needed (like for time-stamped experiments) the different accounts will have a lowercase letter appended on the end (e.g. e10023a, e10023b). When the account is made, the computer department will give you a randomized password for the account.

A.3.1 Passwords

The Linux (or DAQ) password must be changed to a custom one when you login the first time by using the `yppasswd` command. It will ask you to enter the original password and then your new password twice.

A.3.2 Logbooks

Log books are provided by the NSCL and one should be taken from the main-level copy room. Put the date and the experiment number on the cover. It is customary to put on the first page a list of collaborators and the password.

A.3.3 SSH

Many DAQ codes are called from the Data_U machine but actually run on another computer in the experimental vault. Since the codes are trying to communicate with the spdaq machine, it will ask for the password before continuing. This pause in the action will usually cause the desired program call to fail. By setting up a proper `.ssh` directory you can then call these programs without providing a password. In the `/user/monasoft` account is a script that will crate the `.ssh` directory automatically. Copy `auto_ssh.sh` from `/user/monasoft` and run it to do this. There are also directions in the Data_U for setting up the `.ssh` directory to make secure connections to DAQ machines of the same account without passwords.

```
auto_ssh.sh:
#!/bin/bash

### This script will make it such that a password is not necessary
### to ssh into other NSCL machines.
### -Written by WAP
### -Transcribed by GC
### -Quality control by MJS and SMM

cd ~/
chmod 0750 .
rm -rf .ssh
mkdir .ssh
cd .ssh
chmod 0700 .
ssh-keygen -t dsa -P "" -f id_dsa
mv id_dsa.pub authorized_keys
mv id_dsa identity
chmod 0600 identity
chmod 0640 authorized_keys
cd ~/
```

After setting up the `.ssh`, delete the `auto_ssh.sh` from the home directory to keep your home directory clean.

A.3.4 Windows Password Change

The current password for the Windows machine (`u5pc1`) is written on the back page of the MoNA moving log Logbook. The password needs to be changed periodically (every couple of months or so), because of the security settings of the operating system. If prompted to change the password, do so, and write the new password in the MoNA moving log's back page.

A.3.5 Connecting to the outside internet

The data_U machines are only allowed to have an outside connection to the internet (to use www.google.com, etc) with a special proxy. Directions to do this are found on the NSCL Computer Department website: `https://intra.nscl.msu.edu/hd_drupal/faq/internet/proxy`. The basic steps are:

- Open Firefox.
- Go to *Edit* and then *Preferences*.
- Click on the *Advanced* tab.
- Go to the *Network* tab and click on *Settings*.
- Click on *Manual Proxy Settings* and fill in the *HTTP Proxy:* `webproxy.nscl.msu.edu` and *Port: 3128*

- Check the box that says *Use this proxy server for all protocols.* Click OK and close the preferences window and you are good to use Firefox to search the web.

A.4 BASH files

Similar to the `.ssh` directory, some of the programs refer to the standard directory structure (outlined in the next chapter) and are given environment variables within the `.bashrc` file. The standard bash files can be copied from the `/user/monasoft/Dot_files` directory. After logging in with the experiment account, follow these commands. For the first three files, the terminal is going to ask if you want to overwrite; the answer will be yes.

```
> cd ~/
> cp -r /user/monasoft/Dot_files/ .
> cp ~/Dot_files/.bash* .
> cp ~/Dot_files/.g* .
> cp ~/Dot_files/.v* .
> cp ~/Dot_files/.rootrc .
> cp -r ~/Dot_files/.ipython ./
> source ~/.bashrc
> rm -rf ~/Dot_files
```

The important files are the BASH files. There are:

- `.bash_aliases` – for useful aliases of shell commands. Feel free to add any more aliases you would like to this file.

- `.bash_env` – environment variables for BASH...used to source proper directories in spectcl, ROOT, and readout and to use cvs
- `.bashrc` – Configures your BASH environment; sources .bash_aliases and .bash_env on login and sets the BASH prompt.
- `.gvimrc`, `.viminfo`, `.vimrc` – useful files to customize VIM if you so desire
- `.rootrc` – this customizes ROOT so you can use the classes from n2analysis
- `.ipython` – a directory that is add configuration files that add some nice utils for ipython, including some functions that are used by ROOTBeer

A.4.1 event space

When the account was created the computer group should have also issued space on an `event` disk for recording event files. Create a link called `stagearea` to this issued directory.

```
> cd ~/

> mkdir /events/e08016/stagearea

> ln -s /events/e08016/stagearea stagearea
```

Replace `08016` with the proper assigned values issued by the computer group.

A.5 Getting the code from monasoft

There are four classes of codes you need to make an experiment work: readout, an online analysis code (SpecTcl or ROOTBeer), utility codes and settings files, and the trigger logic (xlm).

Computer	System	readout name	command
spdaq34	sweeper	readout-sweeper_caesar	`godaq`
spdaq40	MoNA	readout_mona	`gomonareadout`
spdaq42	LISA	readout_lisa	`golisareadout`

Table A.1: The spdaq machines and corresponding detector systems and readout codes.

A.5.1 Readout

Readout is the code that reads out the data from the respective VMEs and writes this data to disk in a known structure that can be reinterpreted later by an an analysis code.

Because the spdaq machines can handle only so many VMEs being read out to them, MoNA-LISA-Sweeper separates the daq process onto three separate machines necessitating three readout codes and merge the data post-experiment.

A handy (yet incomplete) guide to Ron Fox's Readout code is located in `http://docs.nscl.msu.edu/daq/bluebook/html/`.

Check out all three codes by typing the following commands and entering the password for the monasoft account when prompted[2]:

```
>cd ~/

>cvs checkout readout_mona

>cvs checkout readout_lisa

>cvs checkout readout-sweeper_caesar
```

To make the executables execute the script `make_all.sh` from every `readout_****/skel` directory. Another task the scripts will do is put scripts in the `$HOME/bin` directory that start each readout without needing to be in a specific directory. These scripts (also known as commands) are (for MoNA, LISA, and sweeper) `gomonareadout`, `golisareadout`, and

---

[2] all cvs commands require the monasoft password

`godaq`, respectively.

A.5.1.1 The experiment directory

The readout codes need an `experiment` folder to run properly. Create this by starting either mona or lisa readout. When the ReadoutGui starts up make sure that the Record button is unchecked and then start and stop a run. With this test of Readout, it will automatically make a linked `experiment` directory as well as the subdirectories of `stagearea`: `current`, `orphans`, and `staged`. When Readout runs during the experiment, a folder is made after each run is completed called `run####`.

A.5.2 Online Analysis Code

The NSCL supports the use of SpecTcl for analyzing data. Our group has created a program that uses SpecTcl called spectcl. (Unique, right?) This code has all that is necessary to unpack online data and event files for sweeper, MoNA, and LISA (both separately and merged). If you so choose, this spectcl can be used as the online analysis code.

```
>cd ~/

>cvs checkout spectcl

>cd spectcl/skel

>./make_all.sh
```

You can start spectcl by typing `gospec` in the terminal.

A.5.3 XLM

The XLM controls the trigger logic for MoNA, LISA, and for Level 3.

To check out the XLM

```
>cd ~/
>cvs checkout tools
```

and give the proper password when prompted.

Before the XLM can be used properly, check with Thomas Baumman what the correct and most current bitfiles that are needed. They should be put in `fpga` folder and the `.bash_env` file should have the correct environment variables of bitfiles pointing to the specific ones.

A.5.4 n2analysis

The n2analysis package contains C++ classes and macros to use ROOT for analysis of MoNA-LISA-Sweeper data. It also has the code that unpacks `.evt` files into root files.

To check out this package from the repository, type:

```
>cd ~/
>cvs checkout n2analysis
```

Further instructions on how to make ROOT work are in Sec. A.7.1.

A.5.5 evtMerge

The code that merges event files from timestamping can be checked out by typing:

```
>cd ~/
>cvs checkout evtMerge
```

A.5.6 Using a script to automate the rest

A useful script called `make_homedir.sh`, automates the copying of files from `monasoft` to the home account. Execute this script by typing:

```
>cd ~/
>cp /user/monasoft/make_homedir.sh .
>export THEHOME=$HOME
>./make_homedir.sh
```

The code should be understood, so that if it becomes necessary, someone can diagnose or do by-hand what the script does. I would suggest opening the script to see that you understand what the script does[3].

The script does in order:

- Creates the `bin` directory including sub-bins for 32-bit and 64-bit executables.
- Copies the `SpecTclInit.tcl` and Xamine files for SpecTcl.
- Copies from `monasoft` the following: fpga, noncvstools, and win.
- Checks if you have a `stagearea`.
- Create a sweeper_settings folder in `experiment/current` and links the settings files in the sweeper account so readout-caesar_sweeper can work.
- Create a mona_settings folder in `experiment/current` and links settings files to it.

---

[3] It is also a handy way to learn how BASH scripts work.

A.5.7 the current directory

The contents of the `experiment/current` directory is copied into each `run####` folder. All important setting files for the experiment should be linked to from the `experiment/current` directory. Since the sweeper readout cannot run without the sweeper settings files to be linked, there are two folders created in the current mona_settings and sweeper_settings.

A.6 Setting up Readout

If you haven't made any changes to the experimental set-up, then Readout is properly set-up and you need not do anything else.

A.6.1 MoNA-LISA Settings files

Both MoNA and LISA readout are scripted. That means that TcL scripts configure the hardware that the program readouts out. The critical script to check if anything needs to change in the readout are:

- `****_config_setup.tcl` – Defines the names and locations for the QDC and TDC hardware.
- `****_hardware_run.tcl` – Sets the packet strucutre and initializes the hard ware.
- `****_readout_run.tcl` – Prints the configuration of the Readout.

A.6.2 sweeper readout settings files

Daniel Bazin puts his settings files for all the hardware for the sweeper set-up in the `/user/sweeper/stagearea/current/sweeper_settings` folder. Since these settings files needed to be sourced by readout for every Begin Run, we make links to these files in `stagearea/current`. The script that automates the rest of setting up the account should have made these links already, but you should check that these are correct and if need fix or add these links.

A.7 Online Analysis Codes

A.7.1 ROOTBeer & ROOT

To configure ROOT and the custom classes that allow ROOT to interpret MoNA-LISA data, please do the following:

- Edit the `.rootrc` file so that all references to the account name are correct
- Type in the terminal:

  ```
  >cd ~/n2analysis/src
  >./compile_lib.sh detector hh
  >./compile_lib.sh sweeper cc
  >./compile_lib.sh caesar cc
  >./compile_lib.sh mona cc
  >./compile_lib.sh utils cc
  >./compile_lib.sh unpacker cc
  ```

- Then do: `> make clean`
- `> make`

And now when ROOT starts up is should have the classes defined to be able to read root files of MoNA-LISA data and the evtunpacker should be to unpack `.evt` files.

A.7.2 SpecTcL

Starting spectcl requires that you type `>gospec`. The window files for Xamine are located in `win`.

A.8 Utility Codes

A.8.1 High Voltage Controller

Located in noncvstools/high_volts.

things you should be able to do with the controller

List of important commands

- array loadconfig *.txt - loads an array configuration file. Needs to be done every time the hv controller is started.
- array connect - open TCP connections to the power supplies. If you get `0x0`, then the connection was successful.
- array on/off - turn on/off the whole array
- array importHV fname - Imports HV voltage settings file of new high voltages from gain matching.
- array exportHV fname - Exports the Current HV voltages to a text file for gain matching.

- tube set name volts - Set the tube named name to an integer volts.
- tube on/off name - Turn on/off the named tube.
- tube readV/readI/readP name - Read the current voltage/current/power state of name.

1. To open to the HV controller program, type `HVnewtext`.
2. In the HV controller prompt, type:

   ```
   MoNA HV> array loadconfig MoNA_hv_defs_1007.txt

   MoNA HV> array connect

   MoNA HV> array on

   MoNA HV> array exportHV ../hv_files/Vout_current.tcl

   MoNA HV> end
   ```

   These commands connect the HVcontroller program to the HVmodules, turns on the voltages (if they weren't on already), and exports the current voltages to a file that is readable by the FORTRAN HV fitting code.

1. Now start the HV controller program and connect to the HV modules typing:

   ```
   > HVnewtext

   MoNA HV> array loadconfig MoNA_hv_defs_1007.txt

   MoNA HV> array connect
   ```

2. Now source the new voltage values into the HV channels by typing into the HV controller:

   ```
   MoNA HV> array importHV ../hv_fitting/new_hv_values.txt

   MoNA HV> end
   ```

HV Module	$HVmodule	IP address
MoNA right	caenhv03	35.9.56.157
MoNA left	caenhv02	35.9.56.157
LISA right	lisacaenhv01	35.9.56.178
LISA left	lisacaenhv00	35.9.56.177

Table A.2: The different high voltage modules and their names and IP adresses.

A.8.1.1 Emergency HV control

If the above program does not work, in a pinch you can telnet directly to the computers of each high voltage controller.

Type `> telnet $HVmodule 1527`, where $HVmodule is one of the modules listed in Table A.8.1.1.

A.8.2 HV fitting

The HV fitting folder has the following files:

- class.C – a class file that defines the qdc histograms
- class.h – a class file that has the root files being sourced
- save_hists.C – uses the class to output the histograms of qdcs to a macro file.C
- hvfit.C – functions for fitting — max bin, peak, etc
- run_hvfit.C – macro that runs the fitting routine on file.C for gain matching
- run_qdcfit.C – macro that runs fitting routine on file.C for qdc thresholds
- Edit copy_cosmicruns2root.sh – to copy the evtfiles from stagearea to evtdata and to use the evtunpacker to unpack the evt files to root files.

Consult the Calibrations guide to learn how to use these files.

A.8.3 NSCLDumper

The NSCLDumper is a NSCL supported program that allows for examination of events from online and from event files. To start the nscl buffer dumper go to `/noncvstools/NSCLDumper` and type `>wish NSCLDumper.tcl &`.

Within the same directory is a TcL script that can calculate the total scalers for an event file. To start it, type `wish scalersum.tcl &`.

A.9 Running the experiment

A.9.1 Readout crashing

If a readout or a spdaq machine crashes during a run, the automatic copying and transferring of settings and event files will not happen properly. A properly recorded run creates a run folder, `/experiment/run####`, that contains the two settings folders and a link to the actual .evt file in `/events/e#####/complete`.

To get the links and the Readout program back to working order after a crash first check to see if the spdaq machine needs to be rebooted.

One can reboot the computer remotely when logged in to spdaq from data_U by typing sudo reboot.

```
> ping spdaq##
```

Type `[CTRL]^C` to quit pinging. If there is no response you must go into the N2/N3 vault and reboot the spdaq machine (directions for rebooting are on orange tape on the machine). If the pinging worked or after rebooting spdaq16 make sure there are no Readout codes running. The following command lists the current programs containing ”eadout”.

```
> ps axuww|grep eadout
```

Then kill any programs still running by using the procedure number listed:

```
> kill ####
```

Rebooting the spdaq machine will also kill stray procedures, but requires the user to restart many control programs after.

Follow this check list before continuing with the next run.

1. Restart Readout and manually increase the run number.
2. Start and then stop a run without recording.
3. Use the `>ls -la` command in the `/experiment` directory to look for a run folder (`run####`) made for the interrupted run.
4. Look for copied `mona_settings` and `sweeper_settings` folders within the the run folder.
5. If needed, copy the settings folders into the interrupted run folder:

   ```
   > cd ~/experiment
   > cp -rp /current/mona_settings/ run####/
   > cp -rp /current/sweeper_settings run####/
   ```

6. Now look for a linked .evt file.

   Within the run folder, look for a linked .evt file pointing to the actual .evt file in one of the stagearea subdirectories.

   Look for a linked .evt file in the `experiment/orphans` or `/current` directories.

7. Find the actual .evt file in `stagearea/complete` or `/current` or `/orphan` directories.
8. Move the actual .evt file for the interrupted run into `stagearea/complete`.
9. Fix links to the .evt file for the interrupted run within the `experiment/run####` folder to link to the actual file now located in the `stagearea/complete` directory.

   ```
   > cd ~/experiment/run####
   > ln -s ~/stagearea/complete/run####-4096.evt .
   ```

10. If needed, delete old links from the `experiment/orphans` or `/current` directories.

If all goes well, the next run can now be recorded. Be sure to make a note in the log book during which run the Readout program halted.

A.9.2 Recovering from a reboot

To recover from the reboot, do the following:

1. Restart the CFDs.
2. Restart the XLM. Check XLM.
3. Restart Readout.
4. Restart scalers.
5. Restart online analysis. Attach to spectrodaq.
6. Start run!

A.10 Post-experiment

As the experiment time is completed there a few prudent procedures to perform to ensure the data is capable of being analyzed properly.

A.10.1 Calibration runs

Before turning MoNA-LISA high voltages off, take a couple cosmic background runs for future calibration checks. One long run (6 hours) with MoNA/LISA self-triggered and self-stopped and multiplicity set to "1-fold" and then another long run, again self triggered and stopped, with multiplicity set to "2-fold". The first one can be used to double check the QDC and Xpos calibration. The second run is used to set the T-mean independent offsets for each bar.

A.10.2 Archive tapes

When all the experiment runs and the additional calibration runs are completed, the event files must be copied to tape and then read off the tape into the `evtdata` disk space. The NSCL provides a nice manual for copying data onto tapes called "Preparing to Close your Experimental Account". I will not cover all the directions contained in that manual, so it should be read as well. I will go through the most common steps and address common problems that have arisen in the past.

1. Acquire two LTO or similar digital tapes from the Computer help room. LTO tapes are named by their size in 100 GB (i.e. LTO1 holds 100 GB, etc.). One of the tapes only needs to hold a GB or so, so choose the smallest size available for that one; the other should be large enough to hold all of your event files.

2. Double check that all run folders within the `experiment` directory contain proper links to actual .evt files in the `stagearea/complete` directory.
3. Login to the “tapehost” machine (currently in the Data U. 2 cubicle) with the experimental account.
4. Change directories to the `experiment` directory. `> cd  /experiment`
5. Identify the tape drive you are using. Maybe `/dev/st2` or `/dev/st1`. It is used as the third argument in steps 6 and 9.
6. Record entire `experiment` directory onto tape. `> tar -cvhf /dev/st1 .`
7. Wait for entire directory to be recorded onto the tape (it may take a couple hours). The terminal window should display all items written.
8. Change directories to the `evtdata/e#####` space provided by the computer group. `> cd /evtdata/e#####`
9. Read the files from the tape. `> tar -xvf /dev/st1 .`
10. When the reading is completed, check that the entire `experiment` directory was copied, including actual .evt files (not links).
11. Eject tape and label it with the date, experiment number, and runs included.

If all the `/experiment` run folders were repaired properly if Readout crashed the actual .evt files should have been copied correctly. If they were not copied correctly, find the run folders for the missing .evt files and rewrite the link to the actual .evt file. Then delete the files you just wrote to the `evtdata/e#####` space and start over from step 4.

Since this process copies each .evt file inside their respective `experiment/run####` folders, it is not possible to attach multiple files when analyzing the data with SpecTcl and/or ROOT. A useful trick is to make a new folder within the `/evtdata/e#####` space that contains links to all the .evt files.

```
> cd /evtdata/e#####

> mkdir evt_links

> cd evt_links

> for i in ../run*/*.evt ; do ln -s $i . ; done
```

After you are done, check that all .evt files have a link in this folder.

A.10.3 Analysis Space

Along with an `/evtdata` space the computer group also should have provided a `/projects` space to copy the analysis files. The `/projects` area can be accessed from the high-speed element and fishtank machines, and should be used for all off-line analysis. You will need to transfer the contents of your experimental account's home directory (i.e. `/user/e#####`) to the `/projects` area. It is a good idea to make a tape backup of the home directory area as well; this should be done on a tape separate from the one containing your event files. To do this, use a procedure similar to that outlined in Section A.10.2, except that you will need to specifically exclude the `/experiment` and `/stagearea` directories (since you don't want to copy the event files twice):

1. Change directories to the experimental home directory: `> cd`

2. Record the non event data portion of the home directory onto tape:

   ```
   > tar -cvf /dev/st1 .  --exclude=./experiment --exclude=./stagearea
   ```

3. Change directories to the `projects/e#####` space provided by the computer group:

   ```
   > cd /projects/e#####
   ```

4. Read the files from the tape: `> tar -xvf /dev/st1 .`

5. When the reading is completed, check that the entire `/user/e#####` directory was copied, except for the event files and links to them.

6. Eject tape and label it with the date, experiment number, and directory copied.

Now you have your links pointing to the proper place, and SpecTcl will still be able to read the files once the experimental directory has been deleted. There may still be other links, however, that need to be updated. It is a good idea to scan through all of the subdirectories in your `projects` space to look for any links still pointing to the experimental directory. If you should find any, update them following the same procedure outlined above. Since the subdirectory structure stays the same when you copy all of the files from the experimental home directory to `projects`, you should be able to update the links by simply replacing the `/user/e#####` portion of the file name with `/projects/e#####`.

A.10.4 Executables

Decide where you want the executable for spectcl to go, and make sure to add it to your path. ROOT does not need this, and since all other programs are unusable without a daq, there is no need to change the environment variables.

A.10.5 Managing the changes to the major programs

Before you close the account and tell the computer department that is is okay the delete the account, it is necessary to check to see if any changes to the major codes (readout, spectcl, ROOT) deserved to be put into the cvs repository for use in future experiments.

For each major code (readout_mona, readout_lisa, readout-sweeper_caesar, n2analysis, spectcl, evtMerge, and tools), you will need to go into the directory that houses the code and query the status of the files within the repository. For example, to do this for spectcl, type:

```
>cd ~/spectcl

>cvs status > test.txt
```

This will put the output of the `cvs status` command in the file `test.txt` (which will be a temporary file you will delete afterward). Any files that are shown to be Locally Modified (or even perhaps unknown to the repository) will need to evaluated indiviually if these changes need to commited to the repository. Since this is a complex and detail oriented process, I will omit directions on how to manage change with cvs. Consult any guide on using cvs and consult the groups experts on the program projects before committing any changes.

You will also need to examine if any files that are not in repository (some configuration or utility files) need to be reused in future experiments. Copy any of these into an appropriate folder in `monasoft` that will be copied into the future experiments.

BIBLIOGRAPHY

BIBLIOGRAPHY

[1] G. Audi et al. *Nucl. Phys. A*, 729:3, 2003.

[2] T. Baumann et al. *Nucl. Instr. Meth. A*, 543:517–527, 2005.

[3] M. Belleguic et al. *Nucl. Phys. A*, 682:136c – 142c, 2001.

[4] M. D. Bird et al. *IEEE Trans. Appl. Supercond.*, 15:1252, 2005.

[5] B. A. Brown. private communication, 2009.

[6] B. A. Brown. *Physics*, 3(104), 2010.

[7] B. A. Brown and W. D. M. Rae. NuShell@MSU, 2007.

[8] B. A. Brown and B. H. Wildenthal. *Ann. Rev. Part. Nucl. Sci.*, 38:29, 1988.

[9] Z. Elekes et al. *Phys. Rev. Lett.*, 98:102502, 2007.

[10] N. H. Frank. *Spectroscopy of Neutron Unbound States In Neutron Rich Oxygen Isotopes.* PhD thesis, Michigan State University, 2006.

[11] O. Haxel, J. H. D. Jensen, and H. E. Suess. *Phys. Rev.*, 75:1766, 1949.

[12] C. R. Hoffman. *investigation of the Neutron-rich Oxygen Isotopes at the Drip Line.* PhD thesis, Florida State University, 2009.

[13] C.R. Hoffman et al. *Phys. Rev. Lett.*, 100:152502, 2008.

[14] C.R. Hoffman et al. *Phys. Lett. B*, 672:17–21, 2009.

[15] R. Kanungo et al. *Phys. Rev. Lett.*, 102:152501, 2009.

[16] R. Krücken. Introduction to shell stucture in exotic nuclei. *Contemporary Physics*, 52(2):101–120, 2010.

[17] R. D. Lawson and J. L. Uretsky. *Phys. Rev.*, 108:1300, 1957.

[18] K. Makino and M. Berz. *Nucl. Instr. Meth. A*, 558:346, 2005.

[19] Maria G. Mayer. *Phys. Rev.*, 74(3):235–239, 1948.

[20] Maria G. Mayer. *Phys. Rev.*, 75:1969–1970, 1949.

[21] D. J. Morrissey et al. *Nucl. Instr. Meth. B*, 204:90, 2003.

[22] Alex C. Mueller and Bradley M. Sherrill. *Annu. Rev. Nucl. Part. Sci.*, 43:529–583, 1993.

[23] W. A. Peters. *Study of Neutron Unbound States Using the Modular Neutron Array (MONA).* PhD thesis, Michigan State University, 2007.

[24] C. Rodríguez-Tajes et al. *Phys. Rev. C*, 82(024305), 2010.

[25] H. Scheit. Simple track for MoNA, 2006.

[26] A. Schiller et al. *Phys. Rev. Lett.*, 99:112501, 2007.

[27] D. Sohler et al. *Phys. Rev. C*, 77:044303, 2008.

[28] O. Sorlin and M.-G. Porquet. *Prog. Part. Nuc. Phys.*, 61:602–673, 2008.

[29] M. Stanoiu et al. *Phys. Rev. C*, 69:034312, 2004.

[30] M. Stanoiu et al. *Phys. Rev. C*, 78:034315, 2008.

[31] I. Talmi and I. Unna. *Phys. Rev. Lett.*, 4:469, 1960.

[32] C. Thibault et al. *Phys. Rev. C*, 12(2):644–657, 1975.

[33] P. G. Thirolf et al. *Phys. Lett. B*, 485:16, 2000.

[34] E. K. Warburton, J. A. Becker, and B. A. Brown. *Phys. Rev. C*, 41(3):1147–1166, 1990.

[35] E. K. Warburton and B. A. Brown. *Phys. Rev. C*, 46(3):923–944, 1992.

[36] B. H. Wildenthal. *Prog. Part. Nuc. Phys.*, 11:5, 1984.

[37] B. H. Wildenthal and W. Chung. *Phys. Rev. C*, 22(5):2260–2262, 1980.